UNITED NATIONS EDUCATIONAL, SCIENTIFIC AND CULTURAL ORGANIZATION
INTERNATIONAL ATOMIC ENERGY AGENCY
INTERNATIONAL CENTRE FOR THEORETICAL PHYSICS
I.C.T.P., P.O. BOX 586, 34100 TRIESTE, ITALY, CABLE: CENTRATOM TRIESTE

H4.SMR/984-19

Winter College on Quantum Optics: Novel Radiation Sources

3-21 March 1997

Non-classical light: introduction, generation, applications

S. Solimeno

Dipartimento di Fisica, Università di Napoli, Italy

Properties, generation and applications of non-classical light

Winter College on Quantum Optics : Novel Radiation Sources

Salvatore Solimeno

3-21 March 1997

Squeezed radiation

1.1 P-representation and nonclassical light

1.2 Correlation function and QND measurements

1.3 Correlation functions

1.4 Photo-electron current fluctuations

1.5 Characteristic function formalism

1.5.1 Wigner phase-space density

1.6 Phase-operator

1.7 Minimum-uncertainty states

1.7.1 Squeezed states

1.7.2 Two-photon coherent states

1.7.3 Even and odd coherent states

1.8 Photon number distribution

1.9 Electric field variance

1.10 Multimode squeezed states

1.11 A simple classical model for squeezed harmonic oscillator states

1.11.1 May a parametric process modify the statistics of white noise ?

1.12 Degenerate Optical Parametric Oscillator

1.12.1 Correlation functions

1.13 Open system approach to degenerate OPO

1.13.1 Integration of the equation of motion

1.13.2 Autocorrelation of the sensitivity function

Chapter 2

Detection and generation of vacuum squeezed light by means of a degenerate OPO

2.1 Squeezed state detection

2.1.1 Direct measurement

2.1.2 Homodyne detection

2.1.3 Ordinary homodyne detection

2.1.4 Detector efficiency effects

Balanced homodyne detection

2.1.5 Heterodyne detection

2.2 Gain of a parametric oscillator

2.3 Quantum fluctuations

2.4 Gain measurement

2.5 Control of the cavity length

2.6 Optical Layout

2.6.1 Offset and tilting of an optical component.

Ray matrix of a biconvex matrix

Ray matrix of two prisms

Ray matrix of the input mirror

Cavity ray matrix

Tilting and displacement of the cavity gaussian modes

2.7 Resonance frequencies and parametric gain

2.8 Temperature and length constraints for degenerate operation

2.9 Amplitudes of the modes excited in the cavity

Chapter 3

Interferometric detection of gravitational waves and squeezed radiation

3.1 Introduction

3.2 Quantum input-output theory of a Michelson interferometer

3.3 Multimode Michelson interferometer

3.3.1 Cavity reflection

3.3.2 Output fields

3.4 Interferometer output

3.5 Autocorrelation of the interferometer output

Chapter 1

Squeezed radiation

1.1 P-representation and nonclassical light

Most of the mathematical development of quantum optics to date ha been carried out through the use of a particular set of coherent quantum states for the field

$$|\alpha>=e^{|\alpha|^2/2}\sum_{n=0}^{\infty}\frac{\alpha^n}{\sqrt{n!}}|n>$$

where α is a generally complex parameter which corresponds in the classical limit to the comlex amplitude of a monochromatic field. Although they are not orthogonal to one another , the coherent states form a complete set. These states, which reduce the field correlation functions to factorized forms, offer a convenient basis for the description of fields of all type, as orginally recognized by Roy Glauber[1][2]. In 1963 [3] and Sudarshan[4][5] exhibited a particular form for the density operator ρ which makes it possible to carry out many quantum-mechanical calculations by methods resembling those of classical theory,

$$\rho=\int P(\alpha)\,|\alpha><\alpha|d^2\alpha$$

where $d^2\alpha=d(\Re(\alpha))\,d(\Im(\alpha))$. So doing the field is fully described by the so-called P-representation $P(\alpha)$. In fact, it has been shown that any quantum state of the field may be expanded in terms of functions $P(\alpha)$ in a unique way.

The photon number distribution P_n can be easily derived from $P(\alpha)$ by means of the integral expression

$$\begin{aligned}P_n &= \int P(\alpha)\,|<n|\alpha>|^2 d^2\alpha \\ &= \frac{\exp\left(-|\alpha|^2\right)}{n!}\int P(\alpha)\,|\alpha|^{2n}d^2\alpha\end{aligned}$$

Example 1 *Coherent state:*

$$P(\alpha)=\delta^{(2)}(\alpha-\alpha_0)$$

Example 2 *Chaotic state*

$$P(\alpha)=\frac{1}{\pi\overline{n}}\exp\left(-\frac{|\alpha|^2}{\overline{n}}\right)$$

1.2 Correlation function and QND measurements

variance

It is customary in quantum mechanics to characterize the spread of the measurement of a generic observable A by means of the *variance* defined by

$$V(A) = (\Delta A)^2 = < A^2 > - < A >^2$$

correlation function

More detailed information about he evolution of such measurements is provided by the correlation function

$$< A(t) A(t') >$$

at two times t and $t\prime$. For a statistical system described by the density matrix ρ the correlation function is expressed by the trace of the product $\rho A(t) A(t')$

$$< A(t) A(t') > \Rightarrow < Tr \{\rho A(t) A(t')\} >$$

In general the variance of an observable is a function of time. This fact has strong implications on the repeated meaurement of an observable. In fact, in several case in order to smear out the effects of some noisy sources of errors we measure an observable for a sufficiently long period and finally we average the evolution of these measurements. Now it may happen that the averaging process is in confict with the initial preparation of the system in a state which minimizes the quantum dispersion of the observable.

An important case occurs when we try to measure the position of a mass. From a quantum mechanical point of vieww we are led to prepare at time $t = 0$ the massive system in the eigenstate of the position . This, in turn implies that the momentum variance $V(p)$ is infinite. Thus, when we repeat the measurement of the position after a time interval t, the error in the measurement of $x(t) = x(0) + pt$ becomes infinite, thus vanifying the benefits of a repeated measurement.Such a difficulty arise in the detection of very weak mass displacements produced by gravitational waves.

The above qualitative considerations can be reformulated in a more rigorous way by analizing quantum mechanically the evolution of a generic observable $A(t)$ in the interaction picture. There are situations in which we cannot assume that the act of measurement itself does not degrade the predictability of subsequent measurements. This requirement is satisfied if an observable $A^I(t)$ in the interaction picture commutes with itself at different times,

$$\left[A^I(t), A^I(t')\right] = 0$$

QND observables

This condition ensures that if the system is an eigenstate of $A^I(t)$ it remains in this eigenstatefor all subsequent times although the eigenvalues may change. Such observables are called *QND observables*

Example 3 *free particle*

for a free particle of mass m energy and momentum are QND observables while the position is not. In fact

$$x(t+\tau) = x(t) + p\frac{\tau}{m}$$

so that

$$[x(t+\tau), x(t)] = -i\frac{\hbar\tau}{m}$$

Example 4 *harmonic oscillator*

For a harmonic oscillator

$$\begin{aligned} x(t) &= x(0)\cos\omega t + \frac{p(0)}{m\omega}\sin\omega t \\ p(t) &= p(0)\cos\omega t - m\omega x(0)\sin\omega t \end{aligned}$$

so that

$$\begin{aligned} m\omega\left[x(t), x(0)\right] &= \frac{1}{m\omega}\left[p(t), p(0)\right] = -i\hbar\sin\omega t \\ \left[x(t), p(0)\right] &= \left[p(t), x(0)\right] = i\hbar\cos\omega t \end{aligned}$$

Now, if we introduce the *quadrature phase operators* quadrature phase operators

$$\begin{aligned} X(t) &= \sqrt{\frac{2m\omega}{\hbar}}\left[x(t)\cos\omega t - \frac{p(t)}{m\omega}\sin\omega t\right] \\ Y(t) &= \sqrt{\frac{2m\omega}{\hbar}}\left[x(t)\sin\omega t + \frac{p(t)}{m\omega}\cos\omega t\right] \end{aligned}$$

we see that

$$\begin{aligned} \frac{\hbar}{2m\omega}\left[X(t), X(0)\right] &= \left[x(t)\cos(\omega t) - \frac{p(t)}{m\omega}\sin(\omega t), x(0)\right] \\ &= \cos(\omega t)\left[x(t), x(0)\right] - \frac{\sin(\omega t)}{m\omega}\left[p(t), x(0)\right] \\ &= 0 \end{aligned}$$

In conclusion, the harmonic oscillator admits as QND observables the quadrature phase operators X and Y. This means that the variances of these two operators are time independent

$$\begin{aligned} V\left[X(t)\right] &= V\left(\left[X(0)\right]\right) \\ V\left[Y(t)\right] &= V\left(\left[Y(0)\right]\right) \end{aligned}$$

1.3 Correlation functions

Let us consider a single mode wave of frequency ω and wave vector $\mathbf{k}$, confined to a volume $\mathcal{V}$

$$\begin{aligned} E(\mathbf{r},t) &= i\sqrt{\frac{\hbar\omega}{2\mathcal{V}\varepsilon_0}}\left[a\exp\left[-i(\omega t - \mathbf{k}\cdot\mathbf{r})\right] - a^{+}\exp\left[i(\omega t - \mathbf{k}\cdot\mathbf{r})\right]\right] \\ &= \sqrt{\frac{\hbar\omega}{2\mathcal{V}\varepsilon_0}}\left[X\sin(\omega t - \mathbf{k}\cdot\mathbf{r}) - Y\cos(\omega t - \mathbf{k}\cdot\mathbf{r})\right] \\ &\equiv \underbrace{E^{(+)}(\mathbf{r},t)}_{annihilation\ field} + \underbrace{E^{(-)}(\mathbf{r},t)}_{creation\ field} \end{aligned}$$

where

$$a = \frac{X + iY}{2}$$

In particular, if we indicate by $I(\mathbf{r},t)$ the product

$$I(\mathbf{r},t) = E^{(-)}(\mathbf{r},t)\,E^{+}(\mathbf{r},t)$$

itcan be shown that the photocurrent provided by a photodector with unity quantum efficiency is proportional to[3]

$$\underset{photocurrent}{i(t)} \quad \propto < I(\mathbf{r},t) >$$

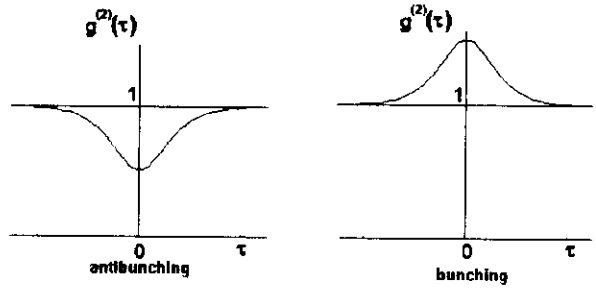

Figure 1.1: Second-order correlation function showing bunching and antibunching

while the correlations among the photocurrents detected at several times are proportional to

$$\begin{aligned} &< \; i(t_1)\, i(t_2) \cdots i(t_n) > \propto <: I(\mathbf{r},t_1)\, I(\mathbf{r},t_2) \cdots I(\mathbf{r},t_n) :> \\ &= \; <: E^{(-)}(t_1)\, E_1^{(-)}(t_2) \cdots E^{(-)}(t_n)\, E^{(+)}(t_n) \cdots E^{(+)}(t_2)\, E^{(+)}(t_1) :> \end{aligned}$$

where $t_1 \leq t_2 \cdots \leq t_n$. In the following we will indicate by $<: \cdots :>$ the expectation value of a time and normal ordered sequence of creation and annihilation operators.

In general for a field represented by the density operator ρ the nth-order correlation function is defined as

$$G^{(n)}_{\mu_1 \cdots \mu_{2n}}(x_1 \cdots x_{2n}) = Tr\left\{\rho E^{(-)}_{\mu_1}(x_1) \cdots E^{(-)}_{\mu_n}(x_n)\, E^{(+)}_{\mu_{n+1}} \cdots E^{(+)}_{\mu_{2n}}\right\}$$

x_j standing for the set of variables t and $\mathbf{r}$

Important informations about the arrival of photons on a detector are contained in the intensity correlation function (seeFig. (1.1)

$$g^{(2)}(t) = \frac{G^{(2)}(t)}{\left[G^{(1)}(0)\right]^2} = \frac{<: I(\mathbf{r},t)\, I(\mathbf{r},0) :>}{<: I(\mathbf{r},0) :>^2} = \frac{Tr\left\{\rho E^{(-)}(t)\, E^{(-)}(0)\, E^{(+)}(0)\, E^{(+)}(t)\right\}}{\left[Tr\left\{\rho E^{(-)}(0)\, E^{(+)}(0)\right\}\right]^2}$$

In particular for $t = 0$ $g^{(2)}(t)$ reduces to

$$\begin{aligned} g^{(2)}(0) &= \frac{< I^2 >}{< I >^2} \\ &= 1 + \frac{< I^2 > - < I >^2}{< I >^2} \\ &= 1 + \frac{V(I)}{< I >^2} \end{aligned}$$

bunching

For classical light the variance of the photocurrent must be positive. However there are situations in which the variance becomes negative , as for example in resonance

antibunching

fluorescence experiments . When $V > 0$ tend to arrive in pairs , so that this situation is referred to as *photon bunching*. On the opposite for $V < 0$ the field exhibit *antibunching* on some time scale: in other words, the arrival of a photon prevents the arrival of a second one within a time interval depending on the time dependence of $g^{(2)}(t)$. The anti-bunching is a typical nonclassical phenomenon .

n-photon state

For example in a n-photon state we have

$$g^{(2)}(0) = 1 - \frac{1}{n}$$

The particular form (??) exhibited for the density operator makes it possible to carry out many quantum mechanical calculations by methods resembling those of classical theory. For example, the second-order correlation function is given by

second-order correlation function

$$g^{(2)}(0) = \frac{G^{(2)}(0)}{\left[G^{(1)}(0)\right]^2} = 1 + \frac{\int P(\alpha)\left[|\alpha|^2 - <|\alpha|>^2\right]^2 d^2\alpha}{\left[\int P(\alpha)|\alpha|^2 d^2\alpha\right]^2}$$

while the variances of X and Y are expressed by

$$\begin{aligned} V(X) &= 1 + \int P(\alpha)\left[\alpha + \alpha^* - <\alpha> - <\alpha^*>\right]^2 d^2\alpha \\ V(Y) &= 1 - \int P(\alpha)\left[\alpha - \alpha^* - <\alpha> + <\alpha^*>\right]^2 d^2\alpha \end{aligned}$$

When $<\alpha> = 0$ (vacuum squeezed radiation) the variances reduce to

$$\begin{aligned} V(X) &= 1 + \int P(\alpha)(\alpha + \alpha^*)^2 d^2\alpha \\ V(Y) &= 1 - \int P(\alpha)(\alpha - \alpha^*)^2 d^2\alpha \end{aligned}$$

For obtaining $\Delta X < 1$ $P(\alpha)$ must take on negative values on the complex α-plane.

1.4 Photo-electron current fluctuations

Let us now discuss a simple model of photodection . If we call T the counting interval

$$i(T;t) = \frac{Ge}{T} n_{pe}(T;t)$$

where G is the gain , e the electron charge and n_{pe} the total number of photon detection events over the counting interval.

The probability $P_n^{(pe)}(t;T)$ for n_{pe} counts in the interval t to $t+T$ is given by

$$P_n^{(pe)}(t;T) = \frac{1}{n!}\left[\eta T \overline{I}(t,T)\right]^n \exp\left[-\eta T \overline{I}(t,T)\right]$$

where η is the quantum efficiency and

$$\overline{I}(t,T) = \frac{1}{T}\int_t^{T+t} I(t')\,dt' = \frac{1}{T}\int_t^{T+t} <: E^{(-)}(t')\,E^{(+)}(t') :> dt'$$

is the mean intensity during the counting interval.Then

$$\overline{i(t)} = \frac{Ge}{T}\overline{n_{pe}(T;t)} = \eta G e \int_t^{T+t} <: E^{(-)}(t')\,E^{+}(t') :> dt'$$

For obtaining the photocurrent spectrum it is necessary to compute the two-time correlation function

$$i(T;0)\,i(T;t) = \left(\frac{Ge}{T}\right)^2 n_{pe}(T;0)\,n_{pe}(T;t)$$

For $t > T$ the probability for $n_{pe}(T;0)$ and $n_{pe}(T;t)$ in the two not-overlapping intervals is equal to the product of probabilities $P_n^{(pe)}(t;T)$. On the other hand when the two intervals overlap partially the joint emission probability does not factorize any more. This problem has ben discussed by Carmichel[6] who has obtained the following result

$$\overline{i(0)\,i(t)} = (\eta Ge)^2 \left[<: \overline{I}(T;0)\,\overline{I}(T;t) :> + \theta(T-t) <: \overline{I}(t-T;0) :>\right]$$

where $\theta(x)$ is the unit step function. In particular, letting $T \to 0$ we have

$$\begin{aligned}\overline{i(0)\,i(t)} &= (\eta Ge\chi)^2 < a^\dagger(0)\,a(0) >^2 \\ &+ \underbrace{\eta\chi(Ge)^2 < a^\dagger(0)\,a(0) > \delta(t)}_{\text{shot noise ontribution}} + \underbrace{(\eta Ge)^2 <: I(0), I(t) :>}_{\text{intensity fluctuations}}\end{aligned}$$

where

$$\chi = \frac{A}{\varsigma_o \hbar\omega}$$

A being the area of the photodetector and ς_o the fre-space impedance.

1.5 Characteristic function formalism

The density oerator is uniquellydetemined by its characteristic function

$$\chi(\eta) = Tr\left\{\rho e^{\eta a^\dagger - \eta^* a}\right\}$$

Introducing now the normallyordered characteristic function

$$\chi_N(\eta) = Tr\left\{\rho e^{\eta a^\dagger} e^{-\eta^* a}\right\}$$

we can easily show that

$$\chi(\eta) = \chi_N(\eta)\, e^{-\frac{1}{2}|\eta|^2}$$

$\chi_N(\eta)$ can be expressed by means of the P representation

$$\chi_N(\eta) = \int e^{\eta\alpha^* - \eta^*\alpha} P(\alpha)\, d^2\alpha$$

Then $\chi_N(\eta)$ is the Fourier transfom of the P representation

1.5.1 Wigner phase-space density

The Wigner function may be defined as the Fourirer transform of the ordered characteristic function $\chi(\eta)$

$$\begin{aligned}W(\alpha) &= \frac{1}{\pi^2}\int e^{\eta^*\alpha - \eta\alpha^*}\chi(\eta)\, d^2\eta \\ &= \frac{1}{\pi^2}\int e^{\eta^*\alpha - \eta\alpha^*} e^{-\frac{1}{2}|\eta|^2}\chi_N(\eta)\, d^2\eta \\ &= \frac{2}{\pi}\int P(\gamma)\, e^{-2|\gamma-\alpha|^2} d^2\gamma\end{aligned}$$

Example 5 *Coherent state*
For a coherent state

$$|\alpha>=|\frac{X+iY}{2}>$$

we have

$$W(X',Y')=\frac{2}{\pi}\exp\left(-\frac{(X-X')^2+(Y-Y')^2}{2}\right)$$

Example 6 *Squeezed state*

For a squeezed state we have

$$W(X',Y')=\frac{2}{\pi}\exp\left(-\frac{(X-X')^2e^{-2r}+(Y-Y')^2e^{2r}}{2}\right)$$

1.6 Phase-operator

Is it possible to measure the phase distribution of a single mode field? It goes without saying that in many cases the phase is the most critical parameter of a field. For example, for discussing the sensitivity of an heterodyne detection scheme it is essential to introduce some sort of measure of the phase. This question was initially addressed by by Dirac without getting to acceptable conclusions. Later , Susskind and Glower [7]introduced the phase operator for a harmonic oscillator

Susskind-Glover phase operator

$$e^{i\phi}_{SG}=\frac{1}{\sqrt{aa^\dagger}}a$$

We immediately observe that such an operator shares the properties of the annihilation operator, whose eigenstates are the coherent states and the number operator. We will see soon, that in analogy with the coherent states, the eigenstates of $e^{i\phi}_{SG}$, although they are not orthogonal one to another, can be used for forming projectors operators $|e^{i\psi}_{SG}><e^{i\psi}_{SG}|d\psi$ which provide a resolution of the identity.

Now, it is easy to show that $e^{i\phi}_{SG}$ has the number state expansion

number state expansion

$$e^{i\phi}_{SG}=\sum_{n=0}^{\infty}|n><n+1|$$

and eigenstates like

$$e^{i\phi}|e^{i\psi}_{SG}>=e^{i\psi}|e^{i\psi}_{SG}>=\sum_{n=0}^{\infty}e^{in\psi}|n>$$

But

$$\left[e^{i\phi}_{Sg},\left(e^{i\phi}_{SG}\right)^\dagger\right]=|0><0|\Rightarrow not\ Hermitian$$

These states provide a resolution of the identity

$$\int|e^{i\psi}_{SG}><e^{i\psi}_{SG}|d\psi=2\pi$$

The phase distribution over the window $-\pi\leq\phi\leq\pi$ for any state is defined by

phase distribution function

$$P_{SG}(\phi)=\frac{|<e^{i\phi}_{SG}|\Psi>|^2}{2\pi}$$

Shapiro [8] has shown that $P_{SG}(\phi)$ provides a correct distribution for optimal phase measurements.

Pegg and Barnett [9]have constructed a family of Hermitian operators, the measurement statistics of which converge, in an appropriate limit, the the phase distribution $P_{SG}(\phi)$. They have considered in a finite subspace of the oscillator Hilbert space the state

$$|\phi_0>=\frac{1}{\sqrt{s+1}}\sum_{n=0}^{s}e^{in\phi_0}|n>$$

with eigenvalue ϕ_0.

$$|\phi_m>=\exp\left(i\frac{2\pi m}{s+1}a^+a\right)|\phi_0>;\ m=0,1,\ldots,s$$

with eigenvalues

$$\phi_m=\phi_0+\frac{2\pi m}{s+1}$$

It is easy to show that the s+1 are mutually orthogonal and form a complete set on the truncated (s+1)-dimensiona Hilbert space.

Pegg-Burnett phase operators

Pegg and Barnett[9] have introduced the Hermitian phase-operator

$$e^{i\phi}_{PB}=\sum_{m=0}^{s}\phi_m|\phi_m><\phi_m|$$

For states restricted to the truncated Hilbert space the measurement statistics of the phase is given by the discrete distribution

$$P_m=|<\phi_m|\Psi>|^2$$

As an example let us consider the phase distribution over the window $-\pi\leq\phi\leq\pi$ for (a) a coherent state , and (b) for a vacuum squeezed state. To this end we have to calculate the projection of the coherent state $|\alpha>$ over the eigenstate $\sum_{n=0}^{\infty}e^{in\phi}|n>$

$$\begin{aligned}<\ e^{i\phi}_{SG}|\alpha>&=\exp\left(-\frac{|\alpha|^2}{2}\right)\sum_{n=0}^{\infty}\frac{e^{-in\phi}\alpha^n}{\sqrt{n!}}\\ =\ \exp\left(-\frac{|\alpha|^2}{2}\right)&\left[\sum_{n=0}^{\infty}\frac{\alpha^n}{\sqrt{n!}}\cos n\phi+i\sum_{n=0}^{\infty}\frac{\alpha^n}{\sqrt{n!}}\sin n\phi\right]\end{aligned}$$

Then (see Fig.??)

$$P_{SG}(\phi)=\frac{\exp\left(-|\alpha|^2\right)}{2\pi}\left[\left(\sum_{n=0}^{\infty}\frac{\alpha^n}{\sqrt{n!}}\cos n\phi\right)^2+\left(\sum_{n=0}^{\infty}\frac{\alpha^n}{\sqrt{n!}}\sin n\phi\right)^2\right]$$

For a vacuum squeezed field we have

$$\begin{aligned}<\ e^{i\phi}_{SG}|S(\varsigma)|0>&=\sum_{n=0}^{\infty}e^{-i2n\phi}<2n|S(\varsigma)|0>\\ =\ \frac{1}{\sqrt{\cosh r}}&\left[\sum_{n=0}^{\infty}\left(\frac{\tanh r}{2}\right)^n\frac{\sqrt{(2n)!}}{n!}\cos 2n\phi+i\sum_{n=0}^{\infty}\left(\frac{\tanh r}{2}\right)^n\frac{\sqrt{(2n)!}}{n!}\sin 2n\phi\right]\end{aligned}$$

so that (see Fig.. 1.2)

$$P_{SG}(\phi)=\frac{1}{2\pi\cosh r}\left[\left(\sum_{n=0}^{\infty}\left(\frac{\tanh r}{2}\right)^n\frac{\sqrt{(2n)!}}{n!}\cos 2n\phi\right)^2+\left(\sum_{n=0}^{\infty}\left(\frac{\tanh r}{2}\right)^n\frac{\sqrt{(2n)!}}{n!}\sin 2n\phi\right)^2\right]$$

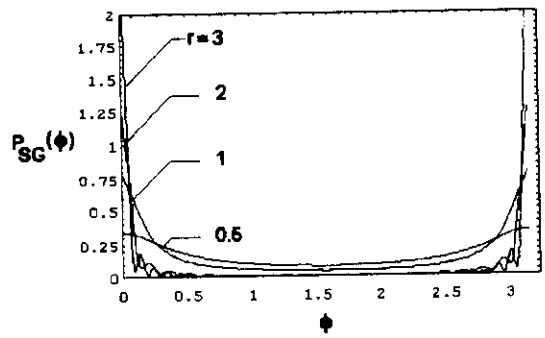

Figure 1.2: Phase distribution for vacuum squeezed states with different values of the squeezing parameter r

1.7 Minimum-uncertainty states

Measurements of quantities by means of light beams are limited by the presence of shot noise. Such anoise limits the resolution of interferometric measurements. In recent years great attention has been paid to the problem of achieving quantum noise reduction beyond the "standard shot noise limit" by using non classical light. In particular, new phase-sensitive detection schemes have been analyzed in the hope of pushing forwardthe sensitivity of gravitational interferometric antennas.

An interferometer is essentially a device for measuring the quadrature phases X,Y of a radiation field,

$$a = \frac{X + iY}{2}$$

Since

$$[X, Y] = 2i\hbar$$

the corresponding uncertainty principle implies

$$\Delta X \Delta Y \geq \hbar$$

All quantum mechanics requires is that the product be bounded from below. In principle one can squeeze ΔX at the expense of stretching ΔY, or vice versa.

The variances of the quadrature phases depend on the state of the field. For example for a coherent field we have

$$\Delta q^2_{coh} = \frac{\hbar}{2\omega} \ , \ \Delta p^2_{coh} = \frac{\hbar\omega}{2}$$

so that the uncertainty product is a minimum

$$(\Delta q \Delta p)_{coh} = \frac{\hbar}{2}$$

1.7.1 Squeezed states

A classical monochromatic field can be represented on the qadrature plane by a vector rotating around the center at the field frequency ω, the vector modulus giving a measure of the field amplitude. Moving to the quantum domain the classical monochromatic field becomes a coherent state $|\alpha\rangle$ of complex amplitude $\alpha = |\alpha|\ e^{i\phi}$. The coherent state is a minimum uncertainty state and in the phase-space it is represented by a round circle centered in α having diameter equal to the square root of the single component variance

$$\Delta X = \Delta Y = 1$$

minimum uncertainty states

There is a whole family of *minimum uncertainty states* defined by

$$\Delta X \Delta Y = 1$$

the coherent state being a special case with $\Delta X = \Delta Y$.

In 1970 Stoler[10][11] demonstrated that in a state of minimum uncertainty product the quadrature phase operators are uncorrelated. This is because a correlation between X and Y would serve as a constraint on the minimization of the uncertianty productand prevent it from attaining its lowest value.

In additon Stoler proved that all the minimum uncertainty packets are unitarily equivalent to the coherent states and that coherence is in fact stationary minimality.

squeeze operator

In conclusion, minimum uncertianty states may be generated from coherent states by using the unitary *squeeze operator*

$$S(\varsigma) = \exp\left(\frac{1}{2}\varsigma^* a^2 - \frac{1}{2}\varsigma a^{\dagger 2}\right)$$

where

$$\varsigma = r\ e^{2i\phi}$$

The squeeze operator obeys the relations

$$S^\dagger(\varsigma) = S^{-1}(\varsigma) = S(-\varsigma)$$

and has the following transformation properties

$$\begin{aligned} S^\dagger(\varsigma)\, a S(\varsigma) &= a\ \cosh r - a^\dagger e^{i2\phi} \sinh r \\ S^\dagger(\varsigma)\, a^\dagger S(\varsigma) &= a^\dagger\ \cosh r - a e^{i2\phi} \sinh r \\ S^\dagger(\varsigma)\,(Y_1 + iY_2)\, S(\varsigma) &= Y_1 e^{-r} + iY_2 e^{r} \end{aligned} \tag{1.1}$$

where

$$X_1 + iY_1 = (X + iY)\, e^{-i\phi}$$

is a rotated complex amplitude. The squeeze operator attenuates one component of the rotated complex amplitude, and it amplifies the other component. The degree of attenuation and amplification is determined by $r = |\varsigma|$, which will be called the *squeeze factor*

squeeze factor

Applying the unitary squeeze operator with complex parameter $\varsigma = r\ e^{i2\phi}$ to the coherent state $|\alpha\rangle$ we get the squeezed state relative to the complex amplitude α. The variances of the new field are no more symmetrically distributed between the quadrature components. Indeed, in the case of real squeezing parameter r, the variance are:

$$\Delta X = \frac{1}{2}\exp(-r)\ ,\ \Delta Y = \frac{1}{2}\exp(r)$$

In the phase-space the circle centered in α become an ellipse with minor axis along X and major in the orthogonal component. The case of complex squeezing

parameter ς corresponds to a transformation of the canonical variables that give compression and expansion along the directions forming the angles ϕ and $\phi + \pi/2$ with the real axis respectively, being 2ϕ the phase of ς.

For $\phi \neq 0$ the variances are given by

$$\begin{aligned}(\Delta X)^2 &= \frac{1}{4}\left\{\exp(-2r)\cos^2(\phi) + \exp(2r)\sin^2(\phi)\right\} \\ (\Delta Y)^2 &= \frac{1}{4}\left\{\exp(-2r)\sin^2(\phi) + \exp(2r)\cos^2(\phi)\right\}\end{aligned}$$

The uncertainty product

$$\Delta X \Delta Y = \sqrt{\cosh^2(2r)\sin^2(2\phi) + \cos^2(2\phi)} \geq 1$$

is minimum only for $\phi = 0, \pi$. These two minimum uncertainty states correspond to real (positive or negative). They are known as "*Quadrature squeezed state*" and "*Phase squeezed state*" (from Phase-space) respectively.

It is worth noting that the variances are independent of the complex amplitude α , so it is possible to look at the squeezed state as a "vacuum squeezed" state of complex amplitude α

$$|\alpha, \varsigma\rangle = D(\alpha)\,|0_\varsigma\rangle = D(\alpha)\,S(\varsigma)\,|0\rangle$$

where

displacement operator

$$D(\alpha) = \exp\left(\alpha a^\dagger - \alpha^* a\right)$$

is the usual *displacement operator.*

Another way of looking at the squeezing come from looking at the field in the space of the photon number and phase operator. The so called "*Amplitude Squeezed state*" or "*number-phase minimum uncertainty state*" features reduced amplitude noise under the *Standard Quantum Limit* (*SQL*). The mean photon number in a quadrature squeezed state is

$$\overline{n}_{\alpha_s} = \left\langle a^\dagger a \right\rangle_{\alpha_s} = |\alpha|^2 + \sinh^2 r$$

while the relative photon noise reads

$$V(n) = |\alpha|^2\left[\cosh(2r) - \sinh(2r)\cos(2\theta)\right] + 2\sinh^2 r \cosh^2 r$$

For $\theta = 0$, that is the squeezing is in phase withthe complex amplitude α, the variance reduces to

$$V(n) = |\alpha|^2 e^{-2r} + 2\sinh^2 r \cosh^2 r$$

The minimum value of $V(n)$ occurs for $e^{6r} = 4|\alpha|^2$ and $V_{\min} = 0.94|\alpha|^{4/3}$.

Now, we note that

$$\frac{V(n) - \overline{n}_{\alpha_s}}{\overline{n}^2_{\alpha_s}} = -\frac{|\alpha|^2 - 2\sinh r \cosh 2r}{2\left(|\alpha|^2 + \sinh^2 r\right)^2}\sinh r$$

For $|\alpha|^2 > 2\sinh r \cosh 2r$ the amplitude squeezed state exhibits a sub-Poissonian photon statistics.

Remark 1 *The squeezed state* $|\alpha, \zeta>$ *is obtained by first squeezing the vacuum and then displacing it*

$$|\alpha, \zeta> = D(\alpha)\,S(\varsigma)\,|0>$$

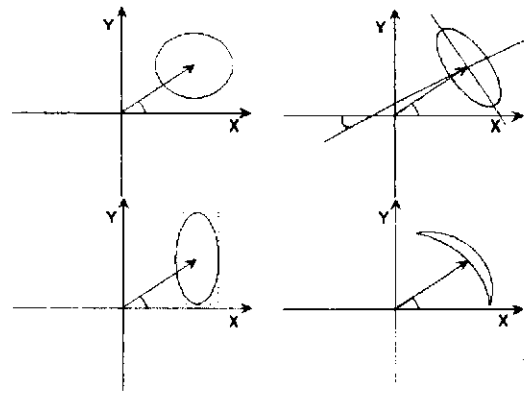

Figure 1.3: Phase-space representation of different squeezed states

1.7.2 Two-photon coherent states

Squeezed states have been defined in an alternative way [?]. Let us introduce a unitary operator which transforms the operator a as

$$UaU^{\dagger} = \mu a + \nu a^{\dagger} \equiv b \tag{1.2}$$

by maintaining the commutation relation

$$\left[b, b^{\dagger}\right] = \hbar$$

Then μ and ν must satisfy the relation

$$|\mu|^2 - |\nu|^2 = 1$$

The eigenstaes of b have been called *two-photon coherent states.*[?]

If we indicate by $|\alpha>_a$ an eigenstate of a , we can express an eigenstate $|\beta>_b$ of b as

$$b|\beta>_b = \beta|\beta>_b = \beta U|\alpha>_a$$

$$|\beta> = D_b(\beta)\,|0>_b$$

where

$$D_b(\beta) = \exp\left(\beta b^{\dagger} - \beta^{*} b\right)$$

and

$$|0>_b = |0>_a$$

$$\begin{aligned} S^{\dagger}(\varsigma)\, a S(\varsigma) &= a\,\cosh r - a^{\dagger} e^{-i2\phi} \sinh r \\ S^{\dagger}(\varsigma)\, a^{\dagger} S(\varsigma) &= a^{\dagger}\,\cosh r - a e^{i2\phi} \sinh r \\ S^{\dagger}(\varsigma)\,(Y_1 + iY_2)\, S(\varsigma) &= Y_1 e^{-r} + iY_2 e^{r} \end{aligned} \tag{1.3}$$

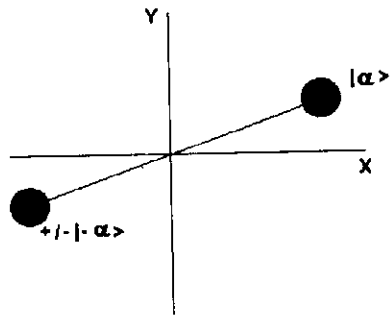

Figure 1.4: Phase-space plots of the uncertainties of even-odd coherent states

It is immediate to prove that the squeeze operator S(ς) satisfies Eq. (??)

$$\begin{aligned} S^{\dagger}(\varsigma)\, aS(\varsigma) &= a\,\cosh r - a^{\dagger}e^{-i2\phi}\sinh r \\ &= \mu a + \nu a^{\dagger} \equiv b \end{aligned}$$

with

$$\begin{aligned} \mu &= \cosh r \\ \nu &= -e^{-i2\phi}\sinh r \end{aligned}$$

1.7.3 Even and odd coherent states

Another class of states reduced uncertainties is obtained by combining linearly two coherent states with opposite complex amplitudes (see Figs. 1.4and ??)

$$\begin{aligned} |\psi > &= |\alpha, \beta_{\pm} > \\ &= N_{\pm}\left(D(\alpha) \pm D(-\alpha)\right)|0, a > \\ &= N_{\pm}\left(|\alpha > \pm|-\alpha >\right) \\ &= e^{|\alpha|^2/2}\sum_{n=0}^{\infty}\frac{\alpha^{2n}}{\sqrt{(2n!)}}|2n > \end{aligned}$$

where + and - signs correspond to "even" and "odd" coherent states, respectively, and their normalization constants are

$$N_{+} = \frac{e^{|\alpha|^2/2}}{2\sqrt{\cosh|\alpha|^2}}\ ,\ N_{-} = \frac{e^{|\alpha|^2/2}}{2\sqrt{\sinh|\alpha|^2}}$$

1.8 Photon number distribution

It can be shown [?] that the squeezed stae $|\alpha, \varsigma >$ has the photon number ditribution

$$P(n) = \frac{1}{n!\mu}\left(\frac{|\nu|}{2\mu}\right)^{n}|H_n\left(\frac{\beta}{\sqrt{2\mu\nu}}\right)|^2 \exp\left(-|\beta|^2 + \frac{\nu}{2\mu}\beta^2 + \frac{\nu^*}{2\mu^*}\beta^{*2}\right)$$

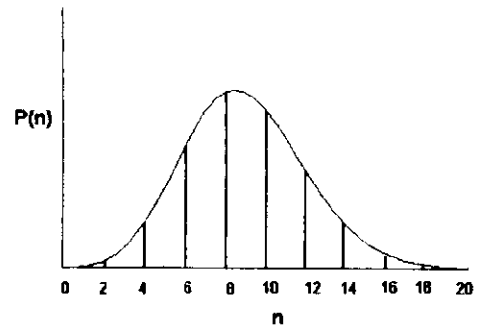

Figure 1.5: Photon number plot for even/odd coherent states

where

$$\begin{aligned}\mu &= \cosh r\,,\\ \nu &= e^{i2\phi}\sinh r\,,\\ \beta &= \mu\alpha+\nu\alpha^{*}=\cosh r\left(1+e^{i2(\phi-\phi_{\alpha})}\tanh r\right)|\alpha|\end{aligned}$$

In particular for $\phi-\phi_{\alpha}=0,\pi$ (see Figs. ?? and ??

$$P(n)=\frac{\exp\left[-(1+\tanh r)\,|\alpha|^{2}\right]}{\cosh r}\frac{1}{n!}\left(\frac{\tanh r}{2}\right)^{n}|H_{n}\left(\frac{1+\tanh r}{\sqrt{2\tanh r}}|\alpha|\right)|^{2}$$

while $\phi-\phi_{\alpha}=\pm\pi/2$

$$P(n)=\frac{\exp\left[-(1-\tanh r)\,|\alpha|^{2}\right]}{\cosh r}\frac{1}{n!}\left(\frac{\tanh r}{2}\right)^{n}|H_{n}\left(i\frac{1-\tanh r}{\sqrt{2\tanh r}}|\alpha|\right)|^{2}$$

In particular, for $r\rightarrow\infty$

$$P(n)=\exp\left[-2|\alpha|^{2}\right]\frac{1}{n!}\frac{1}{2^{n}}|H_{n}\left(\sqrt{2}|\alpha|\right)|^{2}$$

The photon distribution exhibits several oscillations which have been interpreted as interference effects in phase-space[12]

For a vacuum squeezed state the photon number distribution reduces to (see Fig. ??)

$$\begin{aligned}P(2n+1) &= 0\\ P(2n) &= \frac{1}{\cosh r}\frac{1}{(2n)!}\left(\frac{\tanh r}{2}\right)^{2n}|H_{2n}(0)|^{2}=\frac{1}{\cosh r}\left(\frac{\tanh r}{2}\right)^{2n}\frac{(2n)!}{(n!)^{2}}\end{aligned}$$

It is wort noting the absence of odd photon numbers. This is due to the fact that the squeeze operator contain two-photon operators.

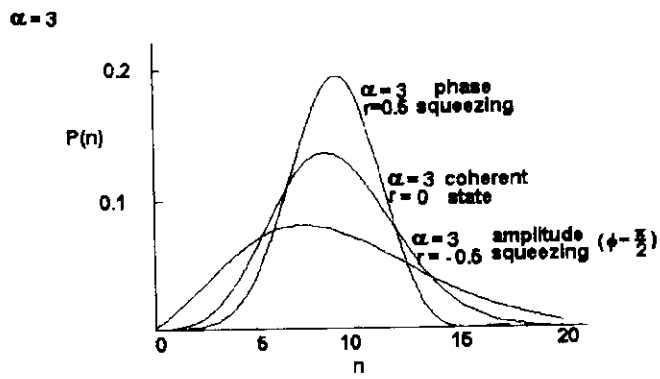

Figure 1.6: Photon number envelope for squeezed states with r=0.5,0,-0.5 and alfa=3.

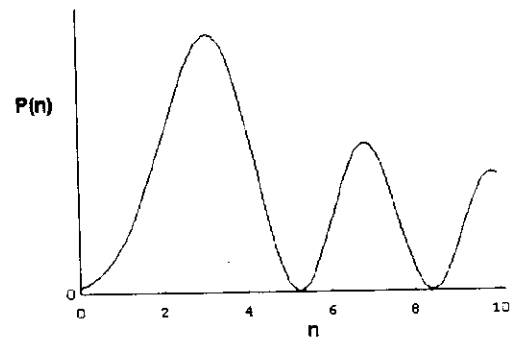

Figure 1.7: Photon number distribution for a squeezed state for r very large and alfa =3

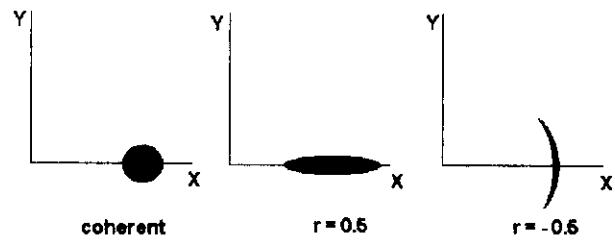

Figure 1.8: Phase-space plots of the uncertainties in a (a) a coherent state, and (b)(c) sqyueezed states with r=0.5 and phase equal to 0 and 90 degrees.

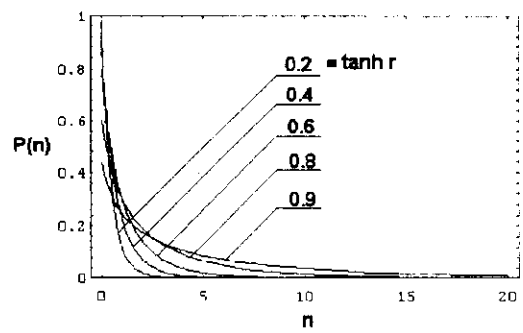

Figure 1.9: Photon number distribution for vacuum squeezed states

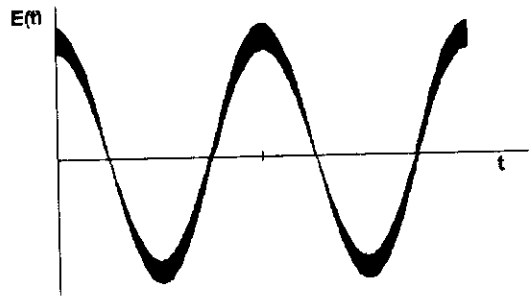

Figure 1.10: Uncertainty in phase and amplitude for squeezed state with reduced phase fluctuations

1.9 Electric field variance

$$E(\mathbf{r},t) = \sqrt{\frac{\hbar\omega}{2\mathcal{V}\varepsilon_0}}\left[X\sin(\omega t - \mathbf{k}\cdot\mathbf{r}) - Y\cos(\omega t - \mathbf{k}\cdot\mathbf{r})\right]$$

The variance of the elecric field is given by

$$V(E(\mathbf{r},t)) = \frac{2\hbar\omega}{\mathcal{V}\varepsilon_0}\left\{V(X)\sin^2(\omega t - \mathbf{k}\cdot\mathbf{r}) + V(Y)\cos^2(\omega t - \mathbf{k}\cdot\mathbf{r}) - V(X,Y)\sin\left[2(\omega t - \mathbf{k}\cdot\mathbf{r})\right]\right\}$$

where

$$V(X,Y) = \frac{<(XY)+(YX)>}{2} - <X><Y>$$

1.10 Multimode squeezed states

Caves and Schumaker[13]have introduced two-mode (labelled b + and -) squeezed states defined by

$$|\alpha_+,\alpha_->= D(\alpha_+)\,D(\alpha_-)\,S^{(2)}(\zeta)\,|0>$$

where $D(\alpha)$ stands for the displacement operator and $S^{(2)}(\zeta)$ is a two-mode squeeze operator

$$S^{(2)}(\zeta) = \exp\left(\zeta^* a_+ a_- - \zeta a_+^\dagger a_-^\dagger\right)$$

where

$$\zeta = re^{i2\phi}$$

The annihilation operators $a_\pm$ are transformed acording to

$$S^{(2)}(\zeta)\,a_\pm S^{(2)\dagger}(\zeta) = a_\pm\cosh r - a_\pm^\dagger e^{i2\phi}\sinh r$$

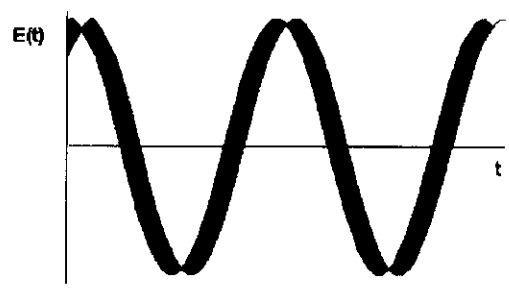

Figure 1.11: Uncertainty in phase and amplitude for a squeezed state with reduced amplitude fluctuations

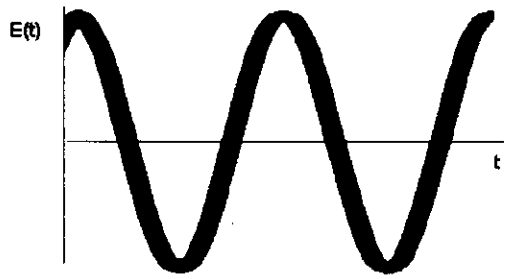

Figure 1.12: Uncertainty in phase and amplitude for a coherent state

thus giving the following epectation values

$$\begin{aligned} < \ a_{\pm} > &= \alpha_{\pm} \\ < \ a_{\pm}a_{\pm} > &= {\alpha_{\pm}}^2 \\ < \ a_{\pm}^{\dagger}a_{\pm} > &= |\alpha_{\pm}|^2 + \sinh^2 r \\ < \ a_{\pm}^{\dagger}a_{\mp}^{\dagger} > &= \alpha_{\pm}^{*}\alpha_{\mp} \\ < \ a_{\pm}a_{\mp} > &= \alpha_{\pm}\alpha_{\mp} - e^{i2\phi}\sinh r \cosh r \end{aligned}$$

The quadrature operator X can be generalized in the two-mode case to

$$X = \frac{a_{+} + a_{+}^{\dagger} + a_{-} + a_{-}^{\dagger}}{\sqrt{2}}$$

and the relative mean and variance are given by

$$\begin{aligned} < \ X > &= 2\Re\left(\alpha_{+} + \alpha_{-}\right) \\ V\left(X\right) &= e^{-2r}\cos^2\phi + e^{2r}\sin^2\phi \end{aligned}$$

1.11 A simple classical model for squeezed harmonic oscillator states

Before discussing the quantum mechanical properties of vacuum squeezed radiation we prefer to introduce a simple classical system made of a mass suspended to a wire of length modulated sinuosoidally. Common life experience tells us that by modulating the length at a frequency twice the natural frequency the system oscillates macroscopically even though it is initially at rest. In addition these oscillations have a well defined phase relation with the length variation .

Put differently this system responds to some external noise, which, in case the frequency of variation of the length is exactly twice the natural one, is amplified . The circumstance that the oscillation is in a well defined phase relation with the length oscillation shows that the system acts as a phase-sensitive amplifier: the components of the white-noise having the right phase are strongly amplified, while the other components are not. Consequently the total amplified noise has a well defined phase relation with the modulating signal.

The systems used in optics for generating squeezed radiaton are substantially similar to the above one. The oscillating mass is replaced by an optical oscillator (i.e. a Fabry-Perot cavity) with resonance frequency modulated by inserting a non-linear crystal . Injecting a pump field the refractive index of the crystal is moduated. If the frequency of the pump is twice the cavity one, we have the so-called degenerate Optical Parametric Oscillator

1.11.1 May a parametric process modify the statistics of white noise ?

Let us consider a suspended mass oscillating at frequency Ω with a damping factor γ. If we modulate the length of the suspension wire at frequeny 2Ω the equation of motion of the mass reads

$$\frac{d^2}{dt^2}s + \gamma\frac{d}{dt}s + \left[\Omega^2 + 2\Omega\kappa\cos\left(2\Omega t\right)\right]s = n\left(t\right) \tag{1.4}$$

where $n(t)$ representing a stationary random force (nose source) and κ is a coefficient measuring the modulation depth of the frequency. By Fourier transforming

$$\begin{aligned} s(t) &= \frac{1}{2\pi}\int_{-\infty}^{\infty} S(\omega)\exp(i\omega t)\,d\omega \\ n(t) &= \frac{1}{2\pi}\int_{-\infty}^{\infty} N(\omega)\exp(i\omega t)\,d\omega \end{aligned}$$

with $S(\omega) = S^*(-\omega)$ and $N(\omega) = N^*(-\omega)$ the transform of Eq. (1.4)reads in proximity of the frequencies $\pm\Omega$

$$(-2x + i\gamma)S(\Omega + x) + \kappa S^*(\Omega - x) = \frac{1}{\Omega}N(\Omega + x) \tag{1.5}$$

where x is a frequency much smaller than Ω . Now, solving with respect to $S(\Omega + x)$ and $S^*(\Omega - x)$ yields

$$\begin{aligned} S(\Omega + x) &= \frac{1}{\Omega}\frac{1}{\Delta_+(x)\Delta_-(x)}\left[(-2x + i\gamma)N(\Omega + x) + \kappa N^*(\Omega - x)\right] \\ S^*(\Omega - x) &= -\frac{1}{\Omega}\frac{1}{\Delta_+(x)\Delta_-(x)}\left[(-2x + i\gamma)N^*(\Omega - x) + \kappa N(\Omega + x)\right] \end{aligned}$$

with

$$\Delta_\pm(x) = -2x + i(\gamma \pm \kappa)$$

thus confirming the above assumption that the spectrum of $s(t)$ be concentrated around $\pm\Omega$

In particular

$$X_\pm(x) = S(\Omega + x) \pm iS^*(\Omega - x) = \frac{1}{\Omega}\frac{N(\Omega + x) \mp iN^*(\Omega - x)}{\Delta_\pm(x)}$$

Since the noise is a stationary random process we have for the correlation function of $N(\omega)$

$$\begin{aligned} \overline{N(\omega)N(\omega')} &= \overline{|N(\omega)|^2}\delta(\omega + \omega') \\ \overline{N(\omega)N^*(\omega')} &= \overline{|N(\omega)|^2}\delta(\omega - \omega') \end{aligned}$$

where the bar indicates the ensembl average. In particular for white noise $\overline{|N(\omega)|^2} \equiv \overline{|N|^2}$ is a quantity independent of the frequency.

Consequently the correlation functions of $S(\Omega + x)$ and $S^*(\Omega + y)$ read

$$\begin{aligned} \overline{S(\Omega + x)S^*(\Omega + y)} &= \sigma_n^2\frac{|2x + i\gamma|^2 + \kappa^2}{|\Delta_-(x)\Delta_-(x)|^2}\delta(x - y) \\ \overline{S(\Omega + x)S(\Omega + y)} &= i\sigma_n^2\frac{2\gamma\kappa}{|\Delta_+(x)\Delta_-(x)|^2}\delta(x + y) \end{aligned}$$

while for $X_+(x)$ and $X_-(x)$ we have

$$\begin{aligned} \overline{X_+(x)X_+(y)} &= i\sigma_n^2\frac{2}{|\Delta_-(x)|^2}\delta(x + y) \\ \overline{X_-(x)X_-(y)} &= -i\sigma_n^2\frac{2}{|\Delta_+(x)|^2}\delta(x + y) \\ \overline{X_+(x)X_+^*(y)} &= \sigma_n^2\frac{2}{|\Delta_-(x)|^2}\delta(x - y) \\ \overline{X_-(x)X_-^*(y)} &= \sigma_n^2\frac{2}{|\Delta_+(x)|^2}\delta(x - y) \\ \overline{X_+(x)X_-(y)} &= \overline{X_+(x)X_-^*(y)} = 0 \end{aligned} \tag{1.6}$$

After these preliminary consideratons about the signal tranform correlations we introduce the low fequency part of the product $\cos(\Omega t+\theta)\, s(t)$

$$\begin{aligned} &< \cos(\Omega t+\theta)\, s(t) >_{lf} \equiv f_\theta(t) \\ &= \Re\left[\exp(-i\theta)\int_{-\infty}^{\infty} S(\Omega+x)\exp(ixt)\,dx\right] \\ &\equiv \int_{-\infty}^{\infty} F_\theta(x)\exp(ixt)\,dx \end{aligned}$$

with $F_\theta(x) = F_\theta^*(-x)$. We can express $F_\theta(x)$ as a suitable combination of functions $X_+(x)$ and $X_-(x)$

$$F_\theta(x) = \frac{1}{2}\left[X_+(x)\left(\exp(-i\theta) - i\exp(i\theta)\right) + X_-(x)\left(\exp(-i\theta) + i\exp(i\theta)\right)\right]$$

In view of Eqs. (1.6)

$$\begin{aligned} \overline{F_\theta(x)\,F_\theta^*(y)} &= \frac{1}{2}\left(1+\sin(2\theta)\right)\overline{X_+(x)\,X_+^*(y)} + \frac{1}{2}\left(1-\sin(2\theta)\right)\overline{X_-(x)\,X_-^*(y)} \\ &= 2\sigma_n^2\frac{(2x)^2+\kappa^2+\gamma^2+\sin(2\theta)\,2\kappa\gamma}{|\Delta_+(x)\,\Delta_-(x)|^2}\delta(x-y) \end{aligned}$$

In particular for $\theta = \pm\pi/4$

$$\begin{aligned} \overline{F_{\pi/4}(x)\,F_{\pi/4}^*(y)} &= 2\sigma_n^2\frac{1}{|\Delta_-(x)|^2}\delta(x-y) \\ \overline{F_{-\pi/4}(x)\,F_{-\pi/4}^*(y)} &= 2\sigma_n^2\frac{1}{|\Delta_+(x)|^2}\delta(x-y) \end{aligned}$$

This in turn implies the spectrum depends critically on the phase θ. When the coupling coefficient κ is very close to the damping coefficient, the spectrum of $f_{\pi/4}(t)$ is almost vanishing with respect to that relative to $f_{-\pi/4}(t)$. On the other hand we also have

$$\overline{f_{\pm\pi/4}^2(t)} = 2\sigma_n^2\int_{-\infty}^{\infty}\frac{1}{|\Delta_\mp(x)|^2}dx = \frac{\pi\sigma_n^2}{\gamma\mp\kappa}$$

In conclusion, if we plot the standard devation of f_θ (radius) versus θ (angular anomaly) we obtain the ellipse shown in Fig. (1.13). The closer κ is to γ the more squeezed is the ellipse.

1.12 Degenerate Optical Parametric Oscillator

The parametric optical amplifier and oscillator (see Fig.1.14) has a long history in quantum optics. The first quantum-mechanical model of this device was proposed by Louisell, Yariv and Siegman [14] in 1961. Later Glauber and Mollow[15][16] used the Glauber P-representation for describing the signal and idler modes.

In recent years this simple dissipative quantum system has been studied by several authors in view of the squeezed-state characteristics of the radiation emitted by a degenerate OPO . Many studies have centered around the calculation of the spectrum of squeezing [17],[18],[19],[20]. Intracavity field statistics have been discussed by Drummond, McNeil and Walls [21] by using the Glauber P-representation, and by Wolinsky and Carmichael [22] by means of the Wigner function. Vyas and Singh have obtained exact analytical expressions [23] for the photon-counting statistics of a degenerate OPO while Kinsler, Fernée and Drummond [24] have investigated the time evolution of squeezingin the signal mode of an undamped parametric amplifier..

Figure 1.13: Polar plot of the standard deviation of f versus the phase theta.

In most of the above works the input laser pump has been treated as a constant amplitude and phase field. On the other hand it is well proved that finite input laser bandwidths alter the output quantum statistics of an intracavity parametric oscillators and amplifiers. In 1972 Crosignani et al studied the effects of pump coherence on frequency conversion and parametric amplification [25] by using a master equation for the P-representation [26]. Some properties of the signal mode in an OPO with time-dependent pump amplitude and phase were studied by Raiford [27] in 1974, without including the stochastic character of the pump field. Wódkiewicz and Zubairy [28] in 1983 have considered the effect of phase and amplitude fluctuations of the pump mode on the quantum-statistical properties of the signal mode in a parametric amplifier by treating classically the pump field and neglecting the pump depletion and the effects of external noise. Drummond and Reid [29] have considered a parametric oscillator above threshold by assuming a classical phase-fluctuating input laser field and treating quantum mechanically the inside pump- and signal-modes . Hillery, Yu and Bergou [30] have considered the consequences of having the pump mode in something other than a coherent state , while Plimak and Walls [31] have analyzed the dynamical restriction to squeezing in a degenerae OPO by using quantum-statistical diagram techniques.

The degenerate parametric oscillator OPO is excited by the classical pump beam E_p

$$E_p(t) = E_{po}e^{-i2\Omega_\ell t - i\alpha} \simeq \eta\, E_{o\ell}^2 e^{-i2\Omega_\ell t \cdot i\alpha} \tag{1.7}$$

obtained by duplicating the laser beam

$$E_\ell(t) = E_{o\ell}e^{\cdot i\Omega_\ell t}$$

with η a real proportionality coefficient.

· The dynamics of the signal mode inside the cavity is ruled in the parametric oscillator approximation by the Hamiltonian

$$H = \hbar\Omega_\ell \hat{a}_s^{\dagger}\hat{a}_s + i\frac{1}{2}\kappa E_{po}\left[\hat{a}_s^2 e^{\cdot i2\alpha} - \hat{a}_s^{\dagger 2}e^{i2\alpha}\right] \tag{1.8}$$

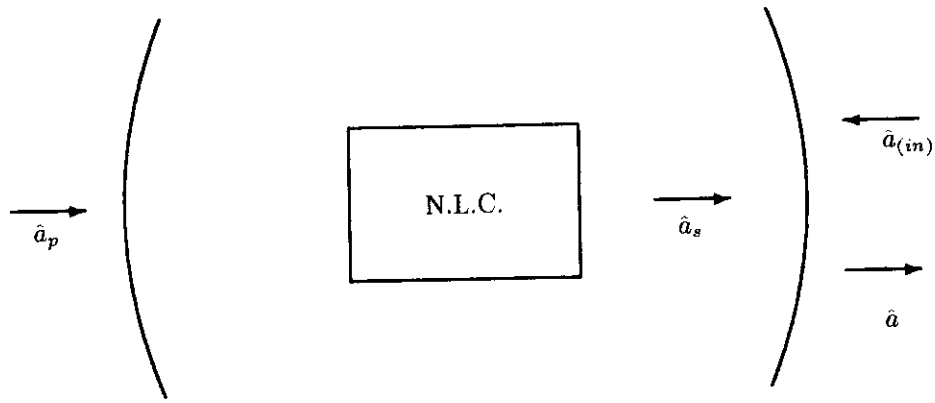

Figure 1.14: OPO cavity. a) N.L.C. → non linear crystal b) $\hat{a}_p$ → pump beam c) $\hat{a}_s$ → signal beam d) $\hat{a}_{in}$ → noise e) $\hat{a}$ → signal output

$\hat{a}$ and $\hat{a}^\dagger$ are field operators transformed to the laser field rotating frame,

$$a \rightarrow e^{i\Omega_\ell t}\hat{a} \ , \ a^\dagger \rightarrow e^{-i\Omega_\ell t}\hat{a}^\dagger \tag{1.9}$$

κ represents the coupling of the pump field wih the OPO. κ depends critically on the phase-matching conditions inside the OPO crystal [32] and on the coupling efficiency of the pump with the cavity.

Integrating the equation of motion of $\hat{a}_s$ relative to the Hamiltonian 1.11 we obtain

$$\hat{a}_s(t) = \hat{a}_s(0)\cosh\beta + \hat{a}_s^\dagger(0)\sinh\beta$$

If we introduce the two quadrature phase amplitudes

$$X_\alpha = e^{-i\alpha}\hat{a} + e^{i\alpha}\hat{a}^\dagger \ , \ Y_\alpha = -ie^{-i\alpha}\hat{a} + ie^{i\alpha}\hat{a}^\dagger$$

we have

$$\begin{aligned} \frac{d}{dt}X_\alpha &= \chi X_\alpha \\ \frac{d}{dt}Y_\alpha &= -\chi Y_\alpha \end{aligned}$$

where

$$\chi = \kappa E_{po}$$

This demonstrates that the parametric amplifier is a phase-sensitive amplifier which amplifies one quadrature and attenuates the other

$$\begin{aligned} X_\alpha(t) &= e^{\chi t}X_\alpha(0) \\ Y_\alpha(t) &= e^{-\chi t}Y_\alpha(0) \end{aligned}$$

The variances satisfy the relations

$$\begin{aligned} V(X_\alpha,t) &= e^{2\chi t}V(X_\alpha,0) \\ V(Y_\alpha,t) &= e^{-2\chi t}V(Y_\alpha,0) \end{aligned}$$

For initial coherent states

$$\begin{aligned} V(X_\alpha,t) &= e^{2\chi t} \\ V(Y_\alpha,t) &= e^{-2\chi t} \end{aligned}$$

1.12.1 Correlation functions

The intensity correlation is equal to

$$g^{(2)}(0;t) = \frac{< \hat{a}_s^\dagger(t)\,\hat{a}_s^\dagger(t)\,\hat{a}_s(t)\,\hat{a}_s(t) >}{< \hat{a}_s^\dagger(t)\,\hat{a}_s(t) >^2}$$

In particular for an an initial vacuum state we have

$$g^{(2)}(t) = 1 + \frac{\cosh 2\chi t}{\sinh^2 \chi t}$$

This indicates that the squeezed light exhibits photon bunching. This means that a squeezed vacuum contains correlated pairs of photons.

For an initial coherent state $||\alpha|e^{i\varphi}>$

$$< \hat{a}_s^\dagger(t)\,\hat{a}_s(t) >= |\alpha^* \cosh\beta + \alpha \sinh\beta|^2 + \sinh^2\beta$$

and

$$\begin{aligned} < \; & \hat{a}_s^\dagger(t)\,\hat{a}_s^\dagger(t)\,\hat{a}_s(t)\,\hat{a}_s(t) >= |\alpha^* \cosh\beta + \alpha \sinh\beta|^4 \\ & +2\sinh\beta|\alpha|^2\left[\sinh\beta\,(2\cosh 2\beta + \cosh\beta) + \cos 2\varphi\,(\sinh\beta \sinh 2\beta + \cosh 2\beta)\right] \\ & +\sinh^2\beta \cosh 2\beta \end{aligned}$$

where $\beta = \chi t$. For $|\alpha|$ large compare with $\sinh^2\beta$ an $\sinh 2\beta$, so that the intensity correlation function evolves as

$$\begin{aligned} < \; & \hat{a}_s^\dagger(t)\,\hat{a}_s^\dagger(t)\,\hat{a}_s(t)\,\hat{a}_s(t) >= e^{4\beta}\left(|\alpha^* + \alpha|^4 + 4|\alpha|^2 + 1\right) \\ < \; & \hat{a}_s^\dagger(t)\,\hat{a}_s(t) >= e^{2\beta}\left(|\alpha^* + \alpha|^2 + 1\right) \end{aligned}$$

$$g^{(2)}(0;t) = \frac{|\alpha^* + \alpha|^4 + 4|\alpha|^2 + 1}{\left(|\alpha^* + \alpha|^2 + 1\right)^2} = 1 - \frac{1}{|\alpha|^2}$$

1.13 Open system approach to degenerate OPO

According to the above model the quadrature component of the OPO signal exhibit opposite exponential growths which would in a very short time to an explosive behavuior. What is unphysical in the above model is the asumption of a lossless signal oscillator.

In addition to the presence of dissipative effects in he OPO cavity the pump field fluctuates as a result of the duplication of a finite linewidth laser beam

$$E_\ell(t) = E_\ell e^{-i\phi_\ell - i\Omega_\ell t} = \left[E_{o\ell} + \delta E_\ell(t)\right] e^{-i\phi_\ell(t) - i\Omega_\ell t}$$

$\delta E(t)$ and $\phi_\ell(t)$ are zero average normal processes. [28]The amplitude fluctuation $\delta E_\ell(t)$ can be described by the Ornstein-Uhlenbeck stochastic process

$$\begin{aligned} \overline{\delta E_\ell(t)} &= 0 \\ \overline{\delta E_\ell(t)\,\delta E_\ell(t')} &= \frac{1}{2}\gamma_{\ell a}\mathcal{N}_{\ell a} e^{-\gamma_{\ell a}|t-t'|} \equiv E_{o\ell}^2 \varepsilon_\ell e^{-\gamma_{\ell a}|t-t'|} \end{aligned}$$

with $\gamma_{\ell a}\mathcal{N}_{\ell a}/2 = E_{o\ell}^2\varepsilon_\ell$ the variance and $\gamma_{\ell a}$ the laser linewidth due to amplitude fluctuations.

The random phase noise $\phi_\ell(t)$ is associated to the instantaneous frequency deviation $\delta\omega_\ell = d\phi_\ell(t)/dt$ from the laser frequency Ω_ℓ, which is in turn described by the process

$$\begin{aligned} \overline{\delta\omega_\ell(t)} &= 0 \\ \overline{\delta\omega_\ell(t)\,\delta\omega_\ell(t')} &= \gamma_{\ell\phi}\delta(t-t') \end{aligned}$$

with $\gamma_{\ell\phi}$ measuring the phase-induced bandwith.

Far above threshold amplitude and phase fluctuations are mutually independent. Accordingly, the instantaneous deviation $\delta\omega_\ell(t)$ and $\delta E_\ell(t)$ will be assumed to be mutually independent stationary processes.

The degenerate parametric oscillator OPO is excited by the classical pump beam E_p, obtained by duplicating the laser beam

$$E_p(t) = [E_{po} + \delta E_p(t)]\, e^{-i2\phi_\ell(t) - i2\Omega_\ell t - i\alpha} \simeq \eta \left[E_{o\ell}^2 + 2E_{o\ell}\delta E_\ell(t)\right] e^{-i2\phi_\ell(t) - i2\Omega_\ell t - i\alpha} \tag{1.10}$$

with η a real proportionality coefficient.

The dynamics of the signal mode inside the cavity is ruled in the parametric oscillator approximation by the Hamiltonian

$$H = \hbar\left[\Omega_\ell + \delta\omega_{cav}(t)\right]\hat{a}_s^\dagger\hat{a}_s + i\frac{1}{2}\kappa(t)\left[E_{po} + \delta E_p(t)\right]\left[\hat{a}_s^2 e^{-i2\phi_\ell(t) - i2\alpha} - \hat{a}_s^{\dagger 2} e^{i2\phi_\ell(t) + i2\alpha}\right] \tag{1.11}$$

where $\delta\omega_{cav}(t)$ stands for the instantaneous deviation of the cavity resonance frequency from Ω_ℓ. $\hat{a}$ and $\hat{a}^\dagger$ are field operators transformed to the laser field rotating frame,

$$a \rightarrow e^{i\Omega_\ell t}\hat{a}\ ,\ a^\dagger \rightarrow e^{-i\Omega_\ell t}\hat{a}^\dagger \tag{1.12}$$

$\kappa(t)$ represents the coupling of the pump field wih the OPO. $\kappa(t)$ depends critically on the phase-matching conditions inside the OPO crystal [32] and on the coupling efficiency of the pump with the cavity.

According to Eq. (??) the signal mode is treated as a randomly modulated hamonic oscillator non-linearly coupled to a driving external field. Implicit in (1.11) is the assumption that the quantities $\delta\omega_{cav}(t), \phi_\ell(t)$ and $\kappa(t)$ vary slowly on the time scale of $T = \Omega_\ell^{-1}$.

The evolution of the vacuum-squeezed field $\hat{a}$ has been derived for a classical coherent pump in Ref. [17] in two steps by integrating first the equation of motion for the signal $\hat{a}_s$ inside the OPO cavity and, later, extending the equation of motion to the external field $\hat{a}_2$ by means of the relation,

$$\hat{a}_2 = \sqrt{2\gamma_{cav}}\hat{a}_s \tag{1.13}$$

representing thc incoming field at the exit mirror and γ_{cav} representing the cavity damping rate, related to the free-spectral-range FSR and the finesse $\mathcal{F}$ (≈ 60) by the relation $\gamma_{cav} = FSR/\mathcal{F}$. The nonlinear crystal of the OPO amplifies, under the action of the pump, the noise a_{in} entering from the input mirror. We will treat a_{in} , as usual, as a stationary gaussian process with vanishing expectation value and δ-type correlation functions [33],

$$< a_{in}^\dagger(t)a_{in}(0) > = < a_{in}(t)a_{in}(0) >= 0$$
$$< a_{in}(t)a_{in}^\dagger(0) >= \mathcal{N}_{in}\delta(t)$$

with $\mathcal{N}_{in}$ a constant depending on the state number density aFor a degenerate OPO operating below threshold $\hat{a}_s$ satisfies the quantum Langevin equation of motion

$$\frac{d\hat{a}_s}{dt} = \gamma_s(t)\, e^{i2\phi_\ell(t) + i2\alpha}\hat{a}_s^\dagger + \left[i\delta\omega_{cav}(t) - \gamma_{cav}\right]\hat{a}_s + \sqrt{2\gamma}\hat{a}_{in} \tag{1.14}$$

Next,

$$\gamma_s(t) = \kappa(t)|E_p(t)| = \eta\kappa(t)|E_\ell(t)|^2$$

$\gamma_s(t)$ depends on the detuning and on the crystal temperature fluctuations and can be assumed equal to[34]

$$\gamma_s(t) \simeq \overline{\gamma_s}\left[1 + 2\frac{\delta E_\ell}{E_{0\ell}} - \left(\frac{\delta T}{\Delta T}\right)^2 - \left(\frac{\delta\omega_{cav}}{\gamma_{cav}}\right)^2\right] \tag{1.15}$$

where $\Delta T \sim .1°C$ stands for the temperature tuning interval ofthe degenerate OPO

We will see in Chapter 3 that the output of an interferometer used for detecting gravitational waves can be expressed as

$$U = \alpha_0 A_{(0)} + A_{(pn)} + (\delta\phi_{(GW)} + \delta\phi_{(sus)} + \delta\phi_{(mir)} + \delta\phi_{(pre)} + \delta\phi_{(rp)})A_{(3)}$$

$.\delta\phi_{(GW)}, \delta\phi_{(sus)}, \delta\phi_{(mir)}, \delta\phi_{(pre)}, \delta\phi_{(rp)}$ represent the dephasing of the two arms of the interferometer due to a gravitational wave ($\delta\phi_{(GW)}$), and the noises introduced by the mirror suspensions ($\delta\phi_{(sus)}$), the mirror vibrations ($\delta\phi_{(mir)}$), the fluctuation of the pressure inside the pipes containing the interferometer arms ($\delta\phi_{(pre)}$) and, finally, the fluctuations due to the radiation pressure effects on the terminal mirrors ($\delta\phi_{(rp)}$).

The operators $A_{(0)}, A_{(pn)}$ and $A_{(3)}$ are defined by

$$\begin{aligned} A_{(0)} &= a_\ell^\dagger a_\ell + a_s^\dagger a_s \\ A_{(pn)} &= e^{i\theta} a_\ell^\dagger a_s + e^{-i\theta} a_s^\dagger a_\ell \\ A_{(3)} &= a_\ell^\dagger a_\ell - a_s^\dagger a_s \end{aligned} \tag{1.16}$$

In particular,the term proportional to $A_{(pn)}$ represents the photon-noise contribution.

In conclusion, the sensitivity of the GW antenna to the photon noise is described by the function

$$h_{pn}\left(|t-t'|\right) \equiv \frac{\overline{<: A_{(pn)}(t), A_{(pn)}(t') :>}}{\overline{|a_\ell|^2}} \tag{1.17}$$

1.13.1 Integration of the equation of motion

Now, redifining the operators[34]

$$\hat{c}_s(t) = \frac{1}{\sqrt{\tilde{\gamma}_s}} \exp\left[\gamma t + i\phi_{cav}(t)\right] a_s(t)$$

with $\phi_{cav}(t) = \int^t \Delta(t')dt'$ and $\tilde{\gamma}_s = \gamma_s \exp\left(i2\phi_\ell + i2\phi_{cav}\right)$ yields

$$\frac{d^2}{dt^2}\hat{c}_s - \varpi^2(t)\,\hat{c}_s = \hat{f}(t) \tag{1.18}$$

with

$$\varpi^2(t) \simeq \overline{\gamma_s}^2 \left[1 + 2\frac{\delta n_\ell}{\overline{n_\ell}} - 2\left(\frac{\delta T}{\Delta T}\right)^2 - 2\left(\frac{\delta\omega_{cav}}{\gamma}\right)^2\right] - 3\left(\delta\omega_\ell - \delta\omega_{cav}\right)^2$$

and

$$\hat{f}(t) = \sqrt{2\gamma}\hat{c}_{(in)}^\dagger$$

In conclusion, the fluctuations of the temperature, cavity length and laser frequency induce a reduction of the effective gain of the OPO.

Since $\delta\omega_\ell$ and $\delta\omega_{cav}$ fluctuate slowly with respect to the characteristic time $1/\gamma_s$, Eq. (1.18) can be integrated by the WKB method,

$$\frac{1}{2\gamma}\begin{bmatrix} \hat{a}_s(t) \\ \hat{a}_s^\dagger(t) \end{bmatrix} = \int_{-\infty}^{t} \begin{bmatrix} \frac{\varpi(t')}{\gamma_s(t')}C + i\frac{\Delta(t')}{\gamma_s(t')}S & e^{i2\phi_\ell(t)}S \\ e^{-i2\phi_\ell(t)}S & \frac{\varpi(t')}{\gamma_s(t')}C - i\frac{\Delta(t')}{\gamma_s(t')}S \end{bmatrix} \cdot \begin{bmatrix} e^{i\Delta\phi_\ell}\hat{a}_{(in)}(t') \\ e^{-i\Delta\phi_\ell}\hat{a}_{(in)}^\dagger(t') \end{bmatrix} dt' \tag{1.19}$$

where

$$\begin{aligned} C(t,t') &= \exp\left[-\gamma\left(t-t'\right)\right]\sqrt{\frac{\gamma_s\left(t\right)\gamma_s\left(t'\right)}{\varpi\left(t\right)\varpi\left(t'\right)}}\cosh\Psi(t,t') \\ S(t,t') &= \exp\left[-\gamma\left(t-t'\right)\right]\sqrt{\frac{\gamma_s\left(t\right)\gamma_s\left(t'\right)}{\varpi\left(t\right)\varpi\left(t'\right)}}\sinh\Psi(t,t') \end{aligned} \tag{1.20}$$

,

$$\Psi(t+\tau,t)=\overline{\varpi}\cdot\tau+\int_t^{t+\tau}\delta\varpi\left(t'\right)dt'\equiv\overline{\varpi}\cdot\tau+\delta\Psi\left(t+\tau,t\right)$$

$\delta\Psi(t+\tau,t)$ being a zero average stationary normal process and

$$\Delta\phi_\ell=\phi_\ell\left(t\right)-\phi_\ell\left(t'\right)$$

1.13.2 Autocorrelation of the sensitivity function

For calculating the average expression of $h_{pn}\left(\tau\right)$ we introduce the functions,

$$\begin{aligned} U\left(t\right) &= \overline{\exp\left(\delta\Psi(t,0)\right)} \\ W(t,\lambda)U(t) &= \overline{\exp\left(\delta\Psi(t,0)+2\delta\Psi(0,\lambda)\right)} \end{aligned}$$

so that,

$$\begin{aligned} h_{pn}\left(\tau\right) &= \mathcal{N}_{in}\overline{\frac{\gamma_s}{\varpi}}\left(1+\varepsilon_{\ell a}e^{-\gamma_{\ell a}\tau}\right)U(\tau) \\ &\times\left[\left(\cos\psi+\overline{\frac{\gamma_s}{\varpi}}\right)\left(\overline{\varpi}-\frac{W'\left(\tau\right)}{2}\frac{1}{1-\frac{\overline{\varpi}}{\gamma_{cav}}}\right)\frac{e^{-(\gamma_{cav}-\overline{\varpi})\tau}}{1-\frac{\overline{\varpi}}{\gamma_{cav}}}\right. \\ &\left.+\left(\cos\psi-\overline{\frac{\gamma_s}{\varpi}}\right)\left(\overline{\varpi}+\frac{W'\left(\tau\right)}{2}\frac{1}{1+\frac{\overline{\varpi}}{\gamma_{cav}}}\right)\frac{e^{-(\gamma_{cav}+\overline{\varpi})\tau}}{1+\frac{\overline{\varpi}}{\gamma_{cav}}}\right] \end{aligned}$$

The function $U\left(\tau\right)$ is defined by

$$U\left(\tau\right)=U_{cav}\left(\tau\right)U_{\ell a}\left(\tau\right)U_{\ell\omega}\left(\tau\right)U_T\left(\tau\right)$$

When the cavity length is well stabilized and the time interval τ is not extremely long, $U_{cav}\left(\tau\right)$ can be approximated by

$$U_{cav}\left(\tau\right)=\overline{\exp\int_0^\tau\delta\varpi_{cav}dt'}\approx 1+\frac{1}{2}\overline{\left(\int_0^\tau\delta\varpi_{cav}dt'\right)^2} \tag{1.21}$$

On the other hand it can be shown that

$$\overline{\left(\int_0^\tau\delta\varpi_{cav}dt'\right)^2}=2\int_0^\infty\frac{\sin^2\left(\frac{\omega\tau}{2}\right)}{\omega^2}S_{\delta\varpi_{cav}}\left(\omega\right)d\omega$$

Since the power spectrum $S_{\delta\varpi_{cav}}\left(\omega\right)$ of $\delta\varpi_{cav}\left(t\right)$ is proportional to that of he intensity output $\delta I_{out}\left(t\right)$, $U_{cav}\left(\tau\right)$ can be derived from experimental measurement of the power spectrum of the fluctuations of the laser beam transmitted through the OPO cavity

In conclusion

$$\begin{aligned} U_{\ell a}(\tau) &\simeq \exp\left[2\pi\varepsilon_\ell \frac{\overline{\gamma_s}^2 \tau}{\gamma_{\ell a}}\left(1-e^{-\gamma_{\ell a}\tau/2}\right)\right] \\ U_{\ell\omega}(\tau) &= \exp\left[\frac{9}{4}\overline{\gamma_s}^2 \frac{\mathcal{N}_{\ell\omega}}{\overline{\gamma_s}^4}\tau\right] \\ U_{cav}(\tau) &= \approx 1+\int_0^\infty \frac{\sin^2\left(\frac{\omega\tau}{2}\right)}{\omega^2} S_{\delta\varpi_{cav}}(\omega)\, d\omega \end{aligned}$$

Since the temperature fluctuations are very slow, we can approximate $U_T(\tau)$ by

$$U_T(\tau) = \exp\left[\tau\overline{\gamma_s}\frac{\delta T^2(0)}{\Delta T^2}\right]$$

Analogous results can be obtained for $W(\tau, t)$.

Bibliography

[1] R. J. Glauber. *Phys. Rev. Lett.*, 10:84, 1963.

[2] R. J. Glauber. Coherent and incoherent staets of theradiation field. *Phys. Rev.*, 131(6):2766–2788, Sep. 1963.

[3] R. J. Glauber. *Quantum Optics and Electronics.* Gordon and Breach, New York, 1964.

[4] E. C. G. Sudarshan. *Phys. Rev. Lett.*, 10:277, 1963.

[5] J. R. Klauder and E. C. G. Sudarshan. *Fundamentals of Quantum Optics.* Benjamin, New York, 1968.

[6] H. J. Carmichael. *J. Opt. Soc. Am.*, B4:1588, 1987.

[7] L. Susskind and J. Glogower. *Physics*, 1:49, 1964.

[8] J. H. Shapiro and S. S. Wagner. Phase and amplitude uncertainties in heterodyne detection. *IEEE J.Q.E.*, QE20:803, 1984.

[9] D. T. Pegg and S. M. Barnett. *Phys. Rev. A*, 39:1665, 1989.

[10] D. Stoler. Equivalence classes of minimum uncertainty packets. *Phys. Rev. D*, 1(12):3217–3219, June 1970. primo lavoro teorico sugli stati squeezed. Stoler has demonstrated the unitary equivalence of all minimum-uncertainty packets to the coherent states. It is of interest to note that in a state of minimum uncertainty product, the position and momentum variables are uncorelated. This is because a correlation between x and p would serve as a constraint on the minimization of the uncertainty product and prevent it from attaining its lowest possible value.

[11] D. Stoler. *Phys. Rev. D*, 4:1935, 1971.

[12] W. Schleich and J. A. Wheeler. *Nature*, 326:574, 1987.

[13] C. M. Caves and B. L. Shoemaker. *Phys. Rev. A*, 31:3068, 1985.

[14] A. Yariv W. H. Louisell and A. Siegman. Quantum fluctuations and noise in parametric processes. *Phys. Rev.*, 124:1646–1654, Dec. 1961.

[15] B. R. Mollow and R. J. Glauber. Quantum theory of parametric amplification. *Phys. Rev.*, 160:1076–1108, Aug. 1967.

[16] B. R. Mollow and R. J. Glauber. *Phys. Rev.*, 160:1097, 1967.

[17] M. J. Collett and C. W. Gardiner. Squeezing of intracavity and traveling-wave light fields produced in parametric amplification. *Phys. Rev. A*, 30(3):1386–1391, Sep. 1984. recent calculations by Milburn and Walls and by Yurke have shown that squeezing in a parametric amplifier is a subject of great subtlety . Milburn and Walls madecalculations using master-equation techniques. The approach presented in this paper povides a method for linking the internal field with the input by identification of the "noise" with the incoming field, and the output is then calculated using the boundary conditions at the cavity mirrors.

[18] M. J. Collett and D. F. Walls. Squeezing spectra for nonlinear optical systems. *Phys. Rev. A*, 32(5):2887–2892, Nov. 1985.

[19] C. W. Gardiner and C.M. Savage. *Opt. Commun.*, 50:173, 1984.

[20] M. Savage and D. F. Walls. *J. Opt. Soc. Am. B*, 4:1514, 1987. calculation of the spectrum of squeezing inside and outside the cavity of an OPO.

[21] P. D. Drummond and M. D. Reid. Laser bandwidth effects on squeezing in intracavity oscillation. *Phys. Rev. A*, 37(5):1806–1808, March 1988.

[22] M. J. Wolinsky and H. J. Carmichel. *Phys. Rev. Lett.*, 60:1836, 1988. the quantum-statistical properties of the intracavity feld of an OPO are described by usingthe positive-P representation.

[23] R. Vyas and Surendra Singh. Phton-countingstatistics of the degenerate optical parametric oscillator. *Phys. Rev.. A*, 40(9):5147–5159, Nov. 1989. it contains exact analytical expresions for the statistics of the OPO.

[24] M. Ferne'e P. Kinsler and P. D. Drummond. Limits to squeezing and phase information in the parametric amplifier. *Phs. Rev. A*, 48(4):3310–3320, Oct. 1993.

[25] U. Ganiel S. Solimeno B. Crosignani, P. Di Porto and A. Yariv. The effect of pump coherence on frequency conversion and parametric. *IEEE J. Quantum Electron.*, QE-8(9):731–739, September 1972.

[26] S. Solimeno A. Yariv B. Crosignani, U. Ganiel. Some consequences of pump coherence on energy exchange in nonlinear optical processes. *Phys. Rev. Lett.*, 27(5):237–239, August 1971.

[27] R. T. Raiford. *Phys. Rev. A*, 9:2060, 1974.

[28] K. Wodkiewicz and M. S. Zubairy. Effect of laser fluctuations on squeezed states in a degenerate parametric amplifier. *Phys. Rev. A*, 27(4):2003–2007, Apr. 1983. fluttuazioni pompa trattata classicamente.

[29] K. J. McNeil P. D. Drummond and D. F. Walls. *Optica Acta*, 28:211, 1980.

[30] Daoqi Yu M. Hillery and Janos Bergou. Effect of the pump state on the behavior of the degenerate parametric amplifier. *Phys. Rev. A*, 49(2):1288–1295, Feb. 1994. la pompa e' trattata quantisticamente.

[31] L I. Plimak and Dan F. Walls. Dynamical restrictions to squeezing in a degenerate optical parametric oscillator. *Phys. Rev. a*, 50(3):2677–2641, Sept. 1994.

[32] G.D. Boyd and D.A. Kleimann. Parametric interaction of focused gaussian light beams. *J. Appl. Physics*, 39:3597, 1968.

[33] C. W. Gardiner. *Handbook of Stochastic Methods.* Springer-Verlag, Berlin, 1st edition, 1985.

[34] A. Porzio R. Romano S. Solimeno M. Fiorentino, P. Maddalena. *Opt. Commun.*, 1996.

Chapter 2

Detection and generation of vacuum squeezed light by means of a degenerate OPO

2.1 Squeezed state detection

2.1.1 Direct measurement

The squeezed state are characterized by two main properties: sub-Poissonian photon number statistics and reduced noise in one of the two quadrature components (phase–squeezing) or in the field amplitude (amplitude–squeezing). The system used to detect these quantum states of light must be able to reveal these characteristic features.

Let's start looking at the simplest system able to detect photon statistic, referred to as a direct detection (see Fig.2.1). In this scheme light having photon number distribution P_n goes directly to a photodetector of quantum efficiency η. The subsequent analysis of the resulting photocurrent provides a measurement of the statistical distribution $P_m(T)$ of the m photon-electrons counted at the detector in the time period T. This distribution is a measure of the light beam statistics disturbed by the non unitary quantum efficiency η. From the mean value and variance of the measured statistic $P_m(T)$ we can infer the photon statistic.

The non unitary efficiency can be modelled by ascribing it to the loss at a beam–splitter with transmittivity $\eta^{\frac{1}{2}} < 1$. Behind the beam splitter there is an ideal photodetector. The annihilation operator a_d at the detector is thus

$$a_d = \sqrt{\eta}a + \underbrace{\sqrt{1-\eta}a_v}_{\substack{vacuum\ field \\ contribution}}$$

where a_v is the vacuum field, having the same frequency ω of the light beam to investigate, entering the other port of the beam splitter. Now we can assume that this field is detected with unitary efficiency (i.e. 100% of the photons are

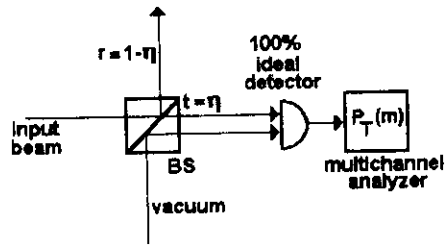

Figure 2.1: Direct measurement scheme of squeezed light photon number distribution

counted). The expectation value of the photon number operator and its variance read respectively [1]

$$\begin{aligned} \langle m \rangle &= \langle n_d \rangle = \left\langle a_d^\dagger a_d \right\rangle = \eta \left\langle a^\dagger a \right\rangle = \eta \langle n \rangle \\ \left\langle (\Delta m)^2 \right\rangle &= \eta^2 \left\langle (\Delta n)^2 \right\rangle + \eta (1-\eta) \langle n \rangle \end{aligned}$$

the non unitary efficiency acts a simple decreasing factor for the respective quantities.

If the measurement period T is negligible compared to the time scale of the fluctuations of the incoming light, as it is for a single mode laser beam, no further distortions are introduced.

Let us imagine that the detected beam is described by $|\alpha, \varsigma\rangle$, obtained from the vacuum state $|0\rangle$ through the action of the displacement operator $D(\alpha)$ and the squeeze operator $S(\varsigma)$ (for a more complete analysis of the photocurrent distribution of direct detection of squeezed light see Ref.[2]).

In the case of large coherent contribution to squeezed state (i.e. $|\alpha| \gg 1$) the mean and the variance of the distribution are

$$\langle m \rangle = \eta |\alpha|^2 \tag{2.1}$$

$$\left\langle (\Delta m)^2 \right\rangle = \eta |\alpha|^2 \left\{ \underbrace{1}_{\text{shot noise}} + \underbrace{\eta \left[\exp(-2r) \cos^2\left(\phi - \frac{1}{2}\theta\right) + \exp(2r) \sin^2\left(\phi - \frac{1}{2}\theta\right) - 1 \right]}_{\text{squeezing}} \right\} \tag{2.2}$$

The unit positive term in the curly bracket gives the usual shot noise contribution of the coherent state $|\alpha\rangle$. The terms in the square bracket, depending on

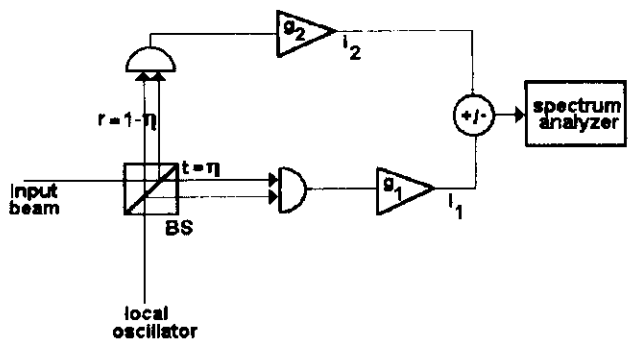

Figure 2.2: Schematic of a homodyne detection scheme

θ and ϕ, are directly connected to the squeezing properties of the light: their sum (the contribution of the square bracket as a whole) is negative if the photon *anti–bunching condition* is satisfied (i.e. the light shows sub–Poissonian statistic) anti-bunching condition

$$\cos(2\phi - \theta) > \tanh r$$

where θ and ϕ respectively represent the phase of the two complex quantities α and ς and $r = \mathrm{Re}(\varsigma)$. So that the antibunching condition for the photon in the light beam leads to a reduction, under the shot noise level, of the variance of the detected number of photons m.

It has to be remarked that the non-classical effect of sub–Poissonian photon statistic is attenuated by the detector efficiency η.

In conclusion, the direct measurement of photon number is able to detect sub-Poissonian statistics, but it is not specifically sensible to he squeezing properties. In alternative we have to consider phase sensitive detection schemes in order to display all squeezing properties.

2.1.2 Homodyne detection

An homodyne detector is based on two equal detectors placed behind the two output ports of a beam splitter. Such a detector can be used in two different configurations depending on the transmission and reflection coefficient of the beam splitter[1]. In particular we will refer respectively to *ordinary homodyne detection* when

$$|r| \ll |t| \tag{2.3}$$

and *balanced homodyne detection* if balanced homodyne detection

$$|r| = |t| = 2^{-\frac{1}{2}} \tag{2.4}$$

[1] ordinary homodyne detection

With reference to Fig.2.2let us consider a lossless beam splitter. Under this assumption the output fields of the beam splitter are obtained by applying a unitary transformation to the input ones

$$\begin{bmatrix} a_{d1} \\ a_{d2} \end{bmatrix} = \begin{bmatrix} r & t \\ t & r \end{bmatrix} \begin{bmatrix} a_L \\ a \end{bmatrix} \tag{2.5}$$

where a_L refer to the local oscillator beam, a to the light beam to detect; r and t are the complex reflection and transmission coefficients for the beam splitter satisfying the relations

$$|r|^2 + |t|^2 = 1 \qquad and \qquad t^* r + r^* t = 0$$

The second condition is satisfied by imposing

$$\arg r - \arg t = \frac{\pi}{2}$$

For complete quantum mechanical treatment of the homodyne detection scheme see Ref.[3][4][5].

2.1.3 Ordinary homodyne detection

In the case of ordinary homodyne detection (2.3) only local oscillator light will reach the second detector so the detected signal is given by the number of photo-electrons provided by the first detector

$$a_{d1}^\dagger a_{d1} = |r|^2 a_L^\dagger a_L + t^* r a^\dagger a_L + r^* t a_L^\dagger a + |t|^2 a^\dagger a \tag{2.6}$$

In homodyne measurements the field and the local oscillator modes have the same frequency and the local oscillator is in a coherent state $|\alpha_L\rangle$. Then the expectation value of $a_{d1}^\dagger a_{d1}$ will read

$$\left\langle a_{d1}^\dagger a_{d1} \right\rangle = |r|^2 |\alpha_L|^2 + 2|r||t||\alpha_L| \langle E_\chi \rangle + |t|^2 \langle a^\dagger a \rangle \tag{2.7}$$

where E_χ is the electric field operator with χ phase term depending on the detector properties

$$E_\chi = \sqrt{\frac{\hbar\omega}{\epsilon_0 V}} \sin kz \left[\exp(i\chi)\, a^\dagger + \exp(-i\chi)\, a\right] \tag{2.8}$$

In the case of homodyne detection the phase χ is

$$\chi = \arg r - \arg t + \phi_L = \frac{1}{2}\pi + \phi_L \tag{2.9}$$

In ordinary homodyne detection (2.3) a strong oscillator is used to satisfy the condition

$$|r||\alpha_L| \gg |t||\alpha| \tag{2.10}$$

with α the complex amplitude of the incoming field. The two conditions (2.3) and (2.10) allow us to simplify 2.7 as

$$\langle n_{d1} \rangle = \underbrace{|r|^2 |\alpha_L|^2}_{\substack{local\ oscillator \\ contribution}} + \underbrace{2|r||t||\alpha_L| \langle E_\chi \rangle}_{\substack{coherent \\ local\ oscillator \\ contribution}} \tag{2.11}$$

Analogously, the photon number variance reads

$$\left\langle (\Delta n_{d1})^2 \right\rangle = |r|^2 |\alpha_L|^2 \left(\underbrace{|r|^2}_{\substack{reflected \\ local\ oscillator \\ contribution}} + \underbrace{4|t|^2 \langle E_\chi^2 \rangle}_{\substack{transmitted \\ field \\ variance}} \right) \tag{2.12}$$

The above two terms arise from the superposition of the reflected local oscillator and the transmitted field variances respectively on to the coherent local oscillator. The ordinary homodyne detection condition (2.3) ensures that the local oscillator contribution is suppressed by the low reflectivity of the beam splitter. While the mean value is dominated by the coherent contribution of the local oscillator field, the number of photon variance is mainly due to the noise in the signal beam [?][6].

2.1.4 Detector efficiency effects

The above analysis of the ordinary homodyne detection scheme doesn't take into account the finite detectors efficiency. Being η this efficiency the mean photocount is

$$\langle m_{d1} \rangle = 2\eta |r| |t| |\alpha_L| \langle E_\chi \rangle = 2\eta |r| |t| |\alpha_L| |\alpha| \cos(\chi - \phi)$$

where the contribution of the local oscillator is supposed to be constant and known and so can be subtracted from the mean value in the (2.11).

The photocurrent variance will read

$$\left\langle (\Delta m_{d1})^2 \right\rangle = \eta |r|^2 |\alpha_L|^2 \left\{ \underbrace{1}_{\substack{shot-noise \\ local\ oscillator}} + \eta |t|^2 \left(4 \langle E_\chi^2 \rangle - 1 \right) \right\} \tag{2.13}$$

For a coherent field the term in the square bracket vanishes and the only remaining term is the shot noise coming from the local oscillator. If the input field is squeezed for the values of χ that satisfy the condition

$$\langle E_\chi^2 \rangle < \frac{1}{4} \tag{2.14}$$

the detected noise is below the shot noise limit, and the field shows sub Poissonian statistic.

By now the homodyne detector gave us the same level of informations of the direct measurement scheme. Further information could be obtained from the local oscillator phase dependence of the input field phase χ (2.9).

The squeezed field variance dependence upon this parameter is easily calculated starting from three quantities: equation (2.8), the value of the mean photon number for a squeezed state $|\alpha,\varsigma\rangle$

$$\langle n\rangle_{\alpha\varsigma} = \langle a^\dagger a\rangle = |\alpha|^2 + \sinh^2 r$$

and the expectation value of a^2 in the same squeezed state

$$\langle a^2\rangle = \alpha^2 - \exp(i\theta)\sinh r\cosh r$$

It has the form

$$\langle {E_\chi}^2\rangle = \frac{1}{4}\left[\exp(-2r)\cos^2\left(\chi - \frac{1}{2}\theta\right) + \exp(2r)\sin^2\left(\chi - \frac{1}{2}\theta\right)\right] \qquad (2.15)$$

and the squeezing condition (2.14) is satisfied for

$$\cos(2\chi - \theta) > \tanh r$$

The final expression of the photocount variance, obtained substituting (2.15) into (2.13), is not very dissimilar from the expression (2.2) obtained by direct measurement of squeezed light with large coherent contribution. The beam splitter in homodyne measurement scheme transforms the input squeezed state in a different squeezed state with larger coherent contribution coming from the local oscillator

$$|\alpha,\varsigma\rangle \longrightarrow |r\alpha_L + t\alpha, t\varsigma\rangle$$

In the ordinary homodyne scheme this new squeezed state is then directly detected. However the mean and the variance detected phase dependence can be studied by varying the local oscillator phase through the relation (2.9). On the contrary the direct detection cannot give any phase information on the squeezing properties of the incoming field. Spanning the local oscillator angle by 2π is possible to span the whole uncertainty ellipse of the squeezed state in the phase-space being the variance value (at fix χ) the projection of the ellipse on to the local oscillator amplitude axis inclined at an angle χ with respect to the quadrature $\widehat{X}$ axis.

In the case of vacuum squeezed state (e.g. coming out from a degenerate OPO operating under oscillation threshold) the field variance in function of the detection angle χ describe a noise band that pulse as the local oscillator phase is varied respect to $\frac{1}{2}\theta$. The variance will get values between $\frac{1}{4}\exp(2r)$ and $\frac{1}{4}\exp(-2sr)$.

Balanced homodyne detection

If the beam splitter parameters satisfy the balance condition (2.4) we are dealing with a different measurement scheme known as balanced homodyne detector. Keeping the same output mode as in (2.5) and the difference signal from the two detector will be determined by the operator

$$a_{d1}^\dagger a_{d1} - a_{d2}^\dagger a_{d2} = i\left(a^\dagger a_L - a_L^\dagger a\right)$$

Using Eqs. (2.8) and (2.9) the mean photon number difference between the two detectors will be

$$\langle n_{12}\rangle = \left\langle a_{d1}^\dagger a_{d1} - a_{d2}^\dagger a_{d2}\right\rangle = 2|\alpha_L|\langle E_\chi\rangle \qquad (2.16)$$

Comparing this result with the expressions (2.11) and (2.7), obtained considering ordinary homodyne detection we see that the balancing procedure has removed the contribution of the local oscillator and the input field alone, keeping only the cross-term. The variance of the detection operator (2.16), assuming that the local oscillator intensity $|\alpha_L|^2$is still much greater than the signal field $|\alpha|^2$, is

$$\left\langle (\Delta n_{12})^2 \right\rangle = 4 |\alpha_L|^2 \langle \Delta E_\chi^2 \rangle$$

This expression must be compared with equation (2.12) referring to the same quantity in the ordinary homodyne detection scheme. In balanced detection the contribution of the local oscillator to the noise has been completely removed [6], and this is the major advantage of the balanced scheme.

Moving to a non-ideal case we have to consider the detector efficiency η, so the mean photocount and its variance will read

$$\begin{aligned} \langle m_{12} \rangle &= 2\eta |\alpha_L| \langle E_\chi \rangle \\ \left\langle (\Delta m_{12})^2 \right\rangle &= \eta |\alpha_L|^2 \left\{ 1 + \eta \left(4 \langle \Delta E_\chi^2 \rangle - 1 \right) \right\} \end{aligned}$$

The above discussion about the photocount variance for ordinary homodyne detection is still valid ; the difference consisting in the different weighting factor of $\langle \Delta E_\chi^2 \rangle$, that is 4η in the balanced case and $4\eta |t|^2$ in the ordinary homodyne.

An experimental analysis of the local oscillator noise suppression in homodyne and heterodyne detection has been carried out [7]by Machida and Yamamoto, who have shown that local oscillator intensity noise can be suppressed to the absolute quantum noise of the detector; the phocount carried on a homodyne detector is not limited by the local oscillator intensity noise.

2.1.5 Heterodyne detection

The heterodyne scheme is ideally to analyze two–mode squeezed light. We suppose that the field has to frequencies centered in ω_0, we indicate this two frequencies as ω_+ and ω_-. The experimental setup of this scheme is analogous to the homodyne detection scheme (see Fig.2.2), in this case we choose the local oscillator frequency $\omega_L = \omega_0$. The current fluctuations spectral component at $\omega = \omega_+ - \omega_L = \omega_L - \omega_-$ will depend upon the contribution of the two excited squeezed modes.

Using a two mode expression for the field in (2.8) of the form

$$E_\chi = \frac{1}{2}\mathcal{E}_{c+} \left[\exp(i\chi)\, a_+^\dagger + \exp(-i\chi)\, a_- \right] + \frac{1}{2}\mathcal{E}_{c-} \left[\exp(i\chi)\, a_-^\dagger + \exp(-i\chi)\, a_- \right]$$

The main problem in heterodyne detection arises from the spectral dependence of the detector efficiency. Only if the two frequencies ω_- and ω_+ are close we can assume equal detection efficiency and the squeezing properties of the field will not be degraded. In this case the measurement results of heterodyne detection will be completely the same obtained for the balance homodyne. This scheme allow to extent the squeezing detection possibility to multi–mode squeezed fields.

The heterodyne scheme can be used also for simultaneous two–quadrature measurements of a signal wave [8].

crystal	*dielectric tensor*	$\lambda\ (\mu m)$	$d_{ijk}\ (\frac{1}{9} \times 10^{-22}\ MKS)$
$LiNbO_3$	*uniaxial*	1.06	$d_{31} = -4.7$
	$n_0 = 2.300\ @300^0 K$		$d_{33} = -27$
	$n_e = 2.208\ @300^0 K$		$d_{22} = 3.2$

Table 2.1: Nonlinear optical coefficients of the litiumniobate

2.2 Gain of a parametric oscillator

We have seen before that a degenerate OPO can generate vacuum squeezed light. In this chapter we will settle for a basic description of parametric amplification in a Fabry-Perot cavity containing a nonlinear crystal.

For field strengths far from the breakdown threshold, the crystal polarization can be expressed in a Taylor series truncated to the third order

$$\begin{array}{rcccc} p_i(t) = & \varepsilon_0 \chi_{ij} e_j(t) & + & 2 d_{ijk} e_j(t) e_k(t) & \\ & \textit{crystal} & & \textit{frequency doubling} & \\ & \textit{anisotropy} & & 3-\textit{wave interactions} & \\ & & & \textit{e.g. parametric process} & \\ + & 4\chi_{ijkl} e_j(t) e_k(t) e_l(t) & & & \\ & 3rd\ \textit{harmonic} & & & \\ & \textit{Raman}-\textit{Brillouin} & & & \\ & self-focusing & & & \\ & \textit{optical wave conjugation} & & & \end{array}$$

where the convention of summing over repreated indices is adopted. The second-order term is responsible for second-harmonic generation, for sum- and difference-frequency generation and for parametric amplification and oscillation.

In the following we will refer uniquely to devices employing $LiNbO_3$. This is a trigonal crystal of class 3m . It is accordingly characterized by a nonlinear susceptitibility matrix of the form[9]

$$d_{ijk} = \begin{bmatrix} 0 & 0 & 0 & 0 & d_{15} & -d_{22} \\ -d_{22} & d_{22} & 0 & d_{15} & 0 & 0 \\ d_{31} & d_{31} & d_{33} & 0 & 0 & 0 \end{bmatrix}$$

Then we have

$$\begin{aligned} p_1 &= \varepsilon_0 n_0^2 e_1 + 2 d_{15} e_1 e_3 - 2 d_{22} e_1 e_2 \\ p_2 &= \varepsilon_0 n_0^2 e_2 - 2 d_{22} e_1^2 + 2 d_{22} e_2^2 + 2 d_{15} e_2 e_3 \\ p_3 &= \varepsilon_0 n_e^2 e_3 + 2 d_{31} e_1^2 + 2 d_{31} e_2^2 + 2 d_{33} e_3^2 \end{aligned}$$

In Table 2.1 we have reported the nonlinear susceptibilities of he $LiNbO_3$ reported in [9] and [10]

Parametric interactions are a particular case of nonlinear optical phenomenons depending on the second order optical susceptibility: This class of phenomenons includes also second harmonic generation and frequency mixing; they all involve

pump signal idler

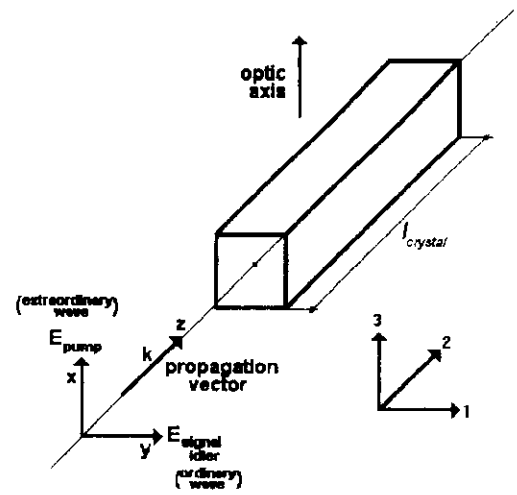

Figure 2.3:

the interaction of three monochromatic fields. In the case of parametric amplification a strong *pump* field of frequency ω_p, a weak *signal* field of frequency ω_s and a weak *idler* field of frequency $\omega_i = \omega_p - \omega_i$ interact in the nonlinear medium, thus giving rise under suitable conditions to amplification of signal and idler.

The relation between the frequencies (*Manley-Rowe relations*) of the three waves,

$$\omega_p = \omega_i + \omega_i$$

is imposed by the conservation of energy and is strictly satisfied when the process is stationary.

To understand the basic features of parametric interaction we will consider the simple case of three collinear plane waves evolving within the nonlinear medium. Referring to [11] for the somewhat lengthy derivation of the equations of evolution for the amplitude of linearly polarized plane waves within the nonlinear medium and we will discuss here only the physical implications of the formula for the variations of the amplitudes of the signal and idler plane waves within the medium as obtained in Ref.. [12].

Let us consider three linearly polarized plane waves propagating along the $z-axis$ of a $LiNbO_3$, with optic axis parallel to $\hat{x}$, of complex amplitudes

$$\begin{aligned} \mathbf{e}_p(z,t) &= \hat{y}\Re\left\{E_p(z)\exp\left[i\omega_p\left(n_p\frac{z}{c}-t\right)\right]\right\} \\ \mathbf{e}_{s,i}(z,t) &= \hat{x}\Re\left\{E_{s,i}(z)\exp\left[i\omega_{s,i}\left(n_{s,i}\frac{z}{c}-t\right)\right]\right\} \end{aligned}$$

Using the conventional notation of calling "3" the optic axis, and "1" and "2"the other two, we have that the pump has only the component E_{p3} while the signal

(idler) has only the component $E_{s,i1}$. Accordingly, the complex amplitude of the crystal polarization is given by

$$\begin{aligned} P_{s,i} &= \varepsilon_0 n_0^2 E_{s,i} + 2d_{15} E_{s,i} E_p \\ P_p &= \varepsilon_0 n_e^2 E_p + 2d_{31} E_{s,i}^2 + 2d_{33} E_p^2 \end{aligned}$$

Plugging these expressions of the polarizations in the Maxwell equations we obtain

$$\begin{aligned} \frac{d}{dz} E_{s,i} &= -\frac{\sigma_{s,i}}{2c\varepsilon_0} E_{s,i} - i\omega_{s,i} d_{15} E_{i,s}^* E_p e^{i(k_p - k_s - k_i)z} \\ \frac{d}{dz} E_p &= -\frac{\sigma_p}{2c\varepsilon_0} E_p - i\omega_p d_{31} E_s E_i e^{-i(k_p - k_s - k_i)z} \end{aligned}$$

where σ represents the crystal losses.

Now, neglecting the pump depletion the variations $\Delta E_{s,i}$ undergone by the signal+idler amplitudes at the crystal exit are given by

$$\Delta E_{s,i} = -i\frac{\omega_s d_{15}}{n_{s,i} c\varepsilon_0} E_p E_{i,s}^* \ell_{xtl} \frac{\sin(\Delta\tilde{k}\ell_{xtl}/2)}{\Delta\tilde{k}\ell_{xtl}/2} \tag{2.17}$$

where ℓ_{xtl} is the length of the nonlinear medium, $n_{s,i}$ is the refractive index. In particular

$$\Delta\tilde{k} = k_p - k_s - k_i + i\frac{\gamma}{\ell_{xtl}} \equiv \Delta k + i\frac{\gamma}{\ell_{xtl}}$$

describes the mismatch of the wave vectors $k_{p,s,i}$ of the three fieds. The damping factor γ represents the attenuation due to the crystal absorption. Although the signal and idler frequencies are roughly coincident it is worth keeping track of a slight difference due to an imperfect degenerate operation f the

Recasting 2.17 in terms of the powers of the waves we have

$$\Delta P_{s,i} = A\omega_{s,i} d_{15} |E_p E_i E_s| \ell_{xtl} \Im\left\{ \frac{\sin(\Delta\tilde{k}\ell_{xtl}/2)}{\Delta\tilde{k}\ell_{xtl}/2} e^{i(\varphi_s + \phi_i - \phi_p)} \right\}|^2 \tag{2.18}$$

"A" representing the beam cross-section area.

perfect phase matching

According to 2.17 the maximum interaction between the three fields occurs when the quantity Δk is zero; this condition is referred to as *perfect phase matching.* where we have introduced explicitly the phases $\phi_{p,s,i}$ of the complex amplitudes $E_{p,s,i}$.

At this stage we are ready to remove the initial assumption of treating the fields as plane waves. In t case of Gaussian beams we must add to the phase delay $\Delta\tilde{k}\ell_{xtl}$ a phase term Ψ typical of the Gaussian beam, which is the outcome of the departure from the propagation along the z-axis. In addition, the field amplitudes undergo large variations in proximity o the waist, which is in or case located at the center of the crystal.[13] These peculiarities bring in a dependence of the power variation in the signal and idler beams by a *focusing parameter*

focusing parameter

$$\zeta = \frac{\ell_{xtl}}{2b}$$

where b is the confocal parameter of the beams (which in general is equal for the three beams as they share the same cavity).

In conclusion Eq. 2.18 is replaced by

$$\Delta P_s = \frac{w_p^2}{8}\omega_s d_{15}|E_p E_s E_i|\ell_{xtl}^2\frac{\pi^2}{\varsigma}|\Im\left\{H(\sigma,\zeta)e^{i(\phi_s+\phi_i-\phi_p)}\right\}|^2$$

where w_p is the pump beam spot size in the waist . Accordingly, switching from plane waves to gassian beams is accounted for by replacing the function

$$\frac{\sin(\Delta\tilde{k}\ell_{xtl}/2)}{\Delta\tilde{k}\ell_{xtl}/2} = \frac{1}{2}\int_{-1}^{1} e^{i\sigma_0 x}dx$$

with $\sigma_0 = \ell_{xtl}\Delta\tilde{k}/2$, by the Boyd and Kleinman [13] function $H(\sigma,\zeta)$

$$H(\sigma,\zeta) = \frac{1}{2\pi}\int_{-\zeta}^{\zeta}\frac{e^{i\sigma x}}{1+ix}dx$$

with

$$\sigma = -b\Delta\tilde{k}$$

the *phase-matching parameter*.. .It is noteworthy that $\Delta\tilde{k}$ is generally complex as a consequence of the crystal absorption losses.However if we neglect the absortion mechanisms, the function $H(\sigma,\zeta)$ becomes real. phase-matching parameter

Until now we have only considered the case of a parametric amplifier without resonating cavities to enhance the gain.

When the nonlinear medium is enclosed in a Fabry-Perot cavity resonating at the three frequencies ω_p, ω_s and ω_i we obtain an optical amplifier or oscillator according whether the parametric gain is less or greater than the cavity damping factor γ_{cav}. The dynamics of this system is described by the Hamiltonian discussed in the last chapter. In particular the coupling coefficient κ can be shown to be related to the properties of the nonlinear crystal by the relation

$$|\kappa|^2 = \frac{\pi c^4\hbar}{V_{cav}\lambda n^3}E_{NL}$$

where E_{NL} is the so called *nonlinear conversion efficiency* (which has the dimensions of the inverse of a power)

$$E_{NL} = \frac{8\pi^2 d_{15}^2}{\varepsilon_0^3 c n_s^2\lambda_s\lambda_i\lambda_p}\ell_{xtl}g(\sigma,\zeta)$$

$\lambda_{p,s,i}$ being the wavelengths of the three fields. In fig. 2.4it. is reported a plot of the function

$$g(\sigma,\zeta) = \frac{\pi^2}{\zeta}\left|\Im\left[H(\sigma,\zeta)\exp\left[i\left(\phi_p-\phi_s-\phi_i\right)\right]\right]\right|^2 \qquad (2.19)$$

against σ in absece of crystal losses and for different values of ζ. (see also Fig. 2.5

A more direct way of characyerizing the OPO is to introduce the *pump threshold input power* (see [14]), that is the minimum pump power needed to operate the OPO as an oscillator pump threshold power

$$P_{pump}^{(in)} = \frac{\pi^2}{4F_s^2 B_p E_{NL}}$$

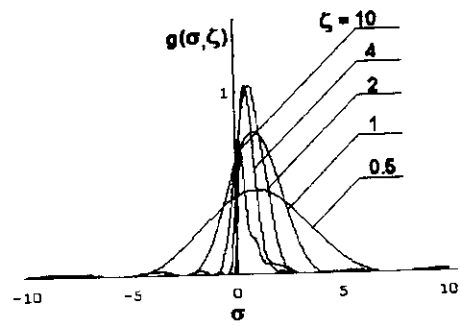

Figure 2.4: Plots of the gain function for different values of the ratio (crystal length)/(cofocal parameter)

where F_s is the finesses of the cavity at the [2]signal and idler frequencies, B_p is the *buildup factor* at the pump frequency (see e.g. [11] for the definition of the above quantities)

buildup factor

nonlinear conversi ciency

In order to achieve a maximum gain (and consequently minimum threshold power) one has to optimize the two parameters σ and ζ. Once the length of the nonlinear medium is chosen ζ can be varied by changing the confocal parameter of the cavity, i.e. by changing its length. To optimize σ one has to change Δk exploiting the characteristics of the nonlinear medium. Being nonlinear optical materials anisotropic, one can then exploit their birefringence and let the three beams propagate through the crystal as ordinary or extraordinary beams. When the pump is an extraordinary ray while signal and idler are ordinary ones, the oscillator is called Type I , in the opposite case one has a Type II oscillator. As the ordinary and extraordinary indices of refraction change with temperature with different rates one may find a temperature for which the phase matching condition is exactly satisfied. For a $LiNbO_3 : MgO$ crystal this temperature ranges between 80 and 110 ^oC,as a function of the concentration of MgO

2.3 Quantum fluctuations

The output field of the OPO is characterized by the amplitude correlation function of the quadrature amplitude

$$X_\chi(t) = e^{-i\chi}\hat{a}(t) + e^{i\chi}\hat{a}^\dagger(t)$$

where the carets indicate that the operators are evaluated in the rotating frame of the subharmonic field,

$$A(\tau;\theta) = <: X_\chi(t), X_\chi(t+\tau) :>$$

[2]nonlinear conversion efficiency

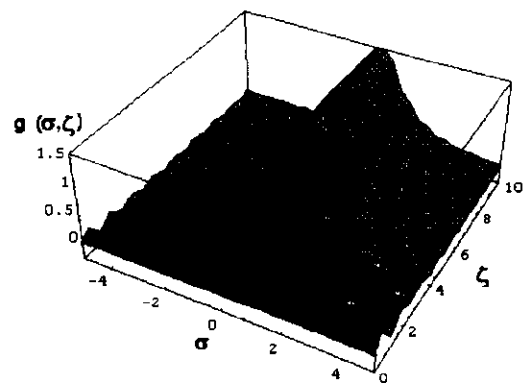

Figure 2.5: 3D plot of the gain versus the detuning parameter and the ratio (cavity length)/(confocal parameter)

If we use a spectrum analyzer for analyzing the squeezed radiation it worth referring to the *spectrum of squeezing* $S(\omega;\theta)$ of the output field, which corresponds to the Fourier transform f the autocorrelation spectrum of squeezing

$$S(\omega;\chi) = 2\gamma \int_{-\infty}^{\infty} A(\tau;\theta)\, e^{-i\omega\tau} d\tau = 4\gamma \int_{-\infty}^{\infty} A(\tau;\theta) \cos\omega\tau d\tau$$

Collett, Gardiner, Savage and Walls[15][16][17] have obtained

$$S_{\pm}(\omega) = \frac{\pm 4\gamma_s |\epsilon_p| \left(\gamma_p^2 + \omega^2\right)}{\left[\gamma_p \left(\gamma_s \mp |\epsilon_p|\right) + |\epsilon_s|^2 - \omega^2\right]^2 + \omega^2 \left(\gamma_s \mp |\epsilon_p| + \gamma_p\right)^2}$$

where $\epsilon_i = \kappa\alpha_i$. The + and - signs refer to conditions of optimum squeezing in one quadrature-phase amplitude. For operation below threshold this equation reduces to

$$S_{\pm}(\omega) = \frac{4E_p/E_p^{thr}}{\left(\omega/\gamma_s\right)^2 + \left(1 \mp E_p/E_p^{thr}\right)^2}$$

2.4 Gain measurement

According to Eq. 2.19 the gain of a degenerate OPO operating as an amplifier (below threshold) depends on the phase difference between the phase of the pump and twice the phase of the signal. Then, once reached the condition of degenerate operation the gain can be obtainded by measuring the amplification undergone by a probe IR beam injected into the cavity (see Fig. 2.7) .By displacing slightly the folding mirrorr the relative phase laser-probe can be varied thus producing a variation of the probe intensity at the exit of the cavity. In Fig. 2.8 it is plotted the probe intensity measured at the cavity exit as a function of time when a sinusoidal voltage was applied to the PZT driving the folding

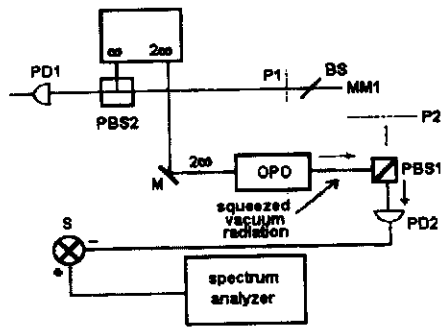

Figure 2.6:

mirror and the condition for degenerate operation was achieved. The gain was simpy obtained by measuring the ratio between the intensity excursion and the intensity in absence of pump.

2.5 Control of the cavity length

In the design of a degenerate parametric oscillator particular attention has to be paid to the cavity locking system in order to achieve simultaneous resonance of the pump, signal and idler. The reader is referred to [12] and [18] for a complete discussion of the constraints to be respected in order to obtain a stable operation of an OPO. It is worth warning that in these references there is not a satisfactory discussion of the (reported) stability of the degenerate OPO. For producing squeezed radiation an additional care has to be paid to the residual fluctuations of the cavity length as they can modify the spectrum of the radiation produced by the OPO [19]. We will here focus on the techniques used to lock cavities which, beyond their use in the OPO, are of wide interest in experimental optics.

These techniques were originally developed to stabilize the frequency of dye lasers using reference cavities , but they can be used as well to lock the length of a cavity to the wavelength of a (stable) laser. These techniques are used whenever one needs to keep a stable and high continuous power circulating within a cavity as in two-photon spectroscopy or continuous second harmonic generation in crystals. The core of a locking scheme is the system which extracts the information relative to the resonance state of the laser within the cavity. This system has to produce an error for the feedback control loop. In proximity of the resonance peak the phase varies linearly with the detuning , thus providing

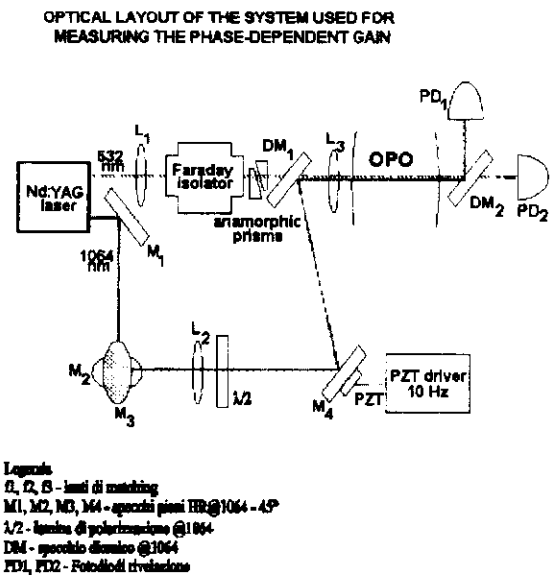

Figure 2.7: Optical layout of the apparatus used for measuring the gain

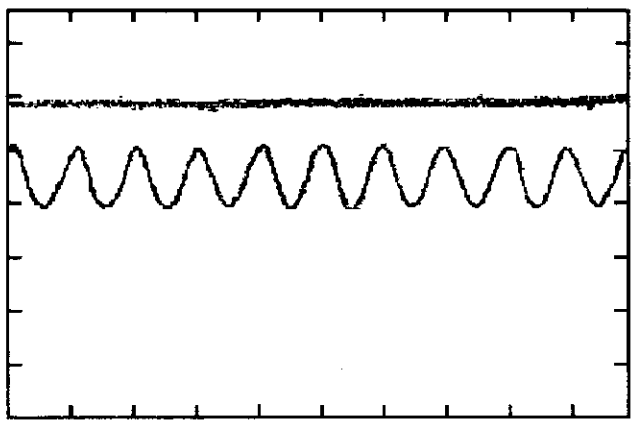

Figure 2.8: Experimental record of the detected signal as a function of time, when an oscillating signal is applied to the PZT controlling the position of the folding mirror.

a good error signal.

The locking schemes differ mainly in the way used to extract the error signal. Initially the locking systems used to monitor the intensity transmitted by the cavity to extract the error signal. A typical plot of the transmitted intensity vs. cavity length showing the classical Airy pattern is reported in fig ??. A common choice was to lock the cavity on the fringe side using as error signal the output of a photodiode measuring the transmitted intensity . This system cannot maximize the circulating power and moreover a perturbation as little as one half of a fringe may carry the cavity out of lock. A more sophisticated approach using the transmitted intensity uses a fast differentiation technique [20].

In Fig ??it is shown the first derivative of the Airy function. As one can see a signal proportional to this derivative would allow to lock the cavity on the maximum of the transmitted intensity thus maximizing the circulating power. The most used derivative technique is the so called mechanical modulation. By means of a PZT the cavity length is modulated sinusoidally at frequency Ω. Consequently the light incident on the photodiode is also modulated; filtering the output one can obtain a sinusoidally modulated signal whose amplitude is proportional to the cavity length.. This information may be recovered by using a lock-in amplifier as shown in fig ?? where a schematic diagram of the mechanical modulation is reported. The main fault of this scheme is that the bandwidth of the control is limited by the value which is no more than a few kHz (and often much less).

To overcome this limit one has to use a fully optical technique; we will here resume two of such schemes which were both introduced by Pound for microwave cavities and then exended to optical cavities by Hansch and Couillaud [21] and by Drever and Hall [22].

The Hansch-Couillaud method is also called polarization spectroscopy scheme. Aschematic of the experimental setup is reported in fig ?? The laser, linearly polarized, is injected in the cavity where is placed a polarizer with its transmission axis forming an angle of 45° with the polarization of the laser. The incoming light may be decomposed into two orthogonal linearly polarized components: of these one is (almost) resonant within the cavity while the other suffers serious losses and is just reflected by the entrance mirror of the cavity. The resonant component is also retroreflected. We report in Fig ?? and ?? the modulus and phase of the reflection coefficient vs. the cavity length and note that the phase is almost linear near the perfect resonance. The polarization spectroscopy technique extracts the information relative to this phase by analizing the polarization of the retroreflected beam , which is a superposition of the resonating and non resonating components. If the cavity is resonant the phase delay between the two components is zero and the retroreflected beam is linearly polarized. This causes balanced outputs of the two photodiodes and the error signal is zero. In case of non-zero delay the retroreflected beam is elliptically polarized; the outputs of the photodiodes are unbalanced and the error signal is different from zero. A plot of the expected error signal vs. cavity length is in fig ??. This scheme may hardly be used to lock a cavity to the laser wavelength expecially if one wants to carry some sort of experiment within the cavity (as in two photon spectroscopy or OPOs). Besides the only bandwidth limitation in this scheme originates from the electronics involved in the detection.

The Drever-Hall technique uses a RF phase modulation of the injected laser

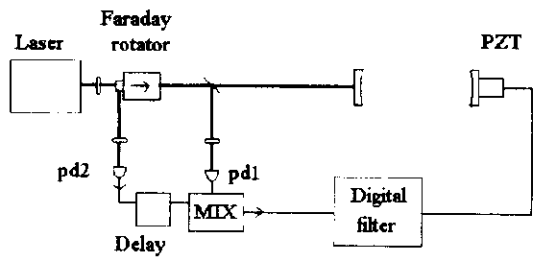

Figure 2.9: Schematic of the Drever-Poundstabilization scheme

beam to extract information about the resonance state of the cavity. The layout of the experimental setup is shown in Fig ??. The laser before passing through a Faraday rotator is phase modulated by an electro-optical modulator (EOM). Phase modulation at frequency Ω adds to the spectrum of the laser a couple of sidebands distant $+\Omega$ and $-\Omega$ by the optical carrier frequency ω. If the carrier is almost resonant with the cavity and the sidebands are well separated (that is to say the frequency Ω is greater than the width of the cavity resonance peak) they will suffer total reflection (see fig ??) and moreover their relative phase will change. The retroreflected beam will then be amplitude modulated and this modulation may be detected by a fast AC photodiode. The signal from the photodiode is demodulated against the RF reference signal driving the EOM. The demodulated signal shows the typical linear shape near the resonance point and is plotted against the cavity length in fig ??. Once again the bandwidth is limited to one half of the modulation frequency, this time however this can be some tens of MHz or more. The Drever-Hall method is very similar to the FM saturation spectroscopy technique used to stabilize gas lasers. In this technique one uses a molecular resonator instead of the cavity. The use of saturation spectroscopy allow to reach sub-Doppler width of molecular lines and the laser may consequently be frequency stabilized with a precision of 1 part over 10^9.

At the end of this rapid survey of the locking techniques we would like to point out the problem of the control networks. In fact once one has extracted the error signal it is often necessary to further elaborate the signal before closing the feedback loop in order to satisfy the stability conditions. Generally analog feedback networks are used. There is however a growing interest in digital networks. This approach is more flexible than the analog one and is very useful in systems with a large number of controlled variables.[20]. In Figs. ?????? we have reported some typical spectra measured on a digitally controlled apparatus.

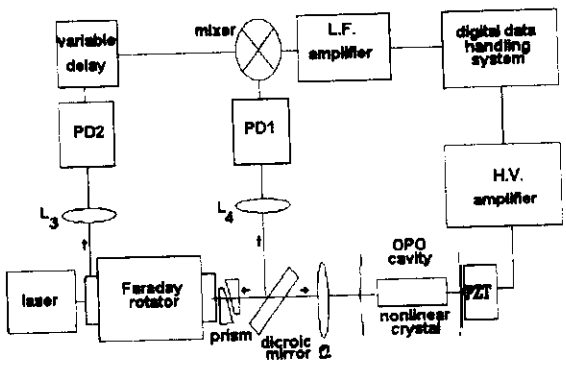

Figure 2.10: Layout of the cavity length control system

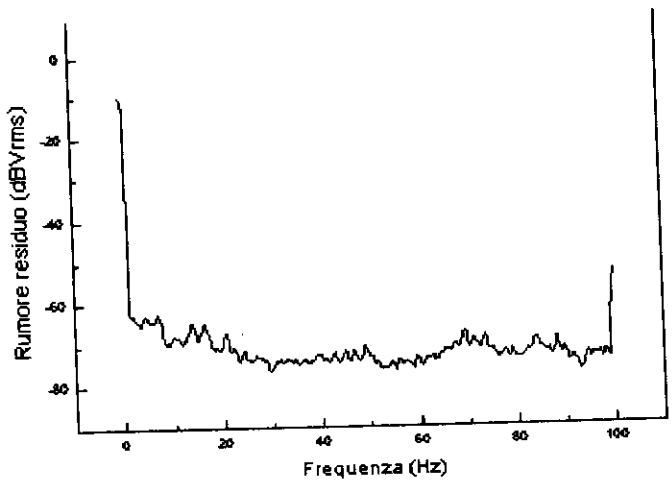

Figure 2.11: Spectrum of the cavity length fluctuations in the range 0-100 Hertz

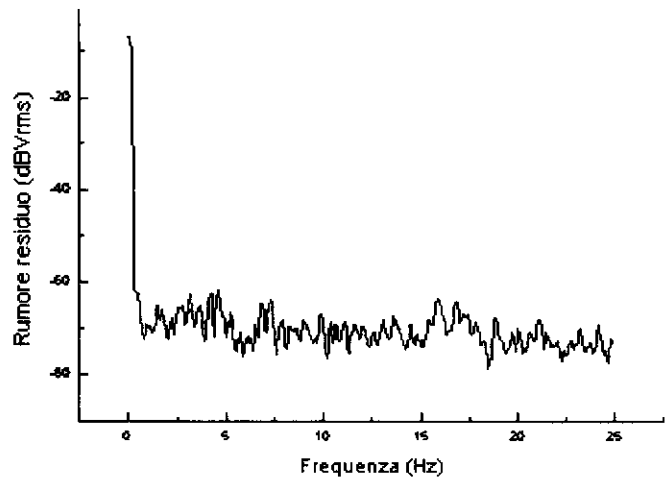

Figure 2.12: Spectrum of the cavity fluctuations in the range 0-25 Hz

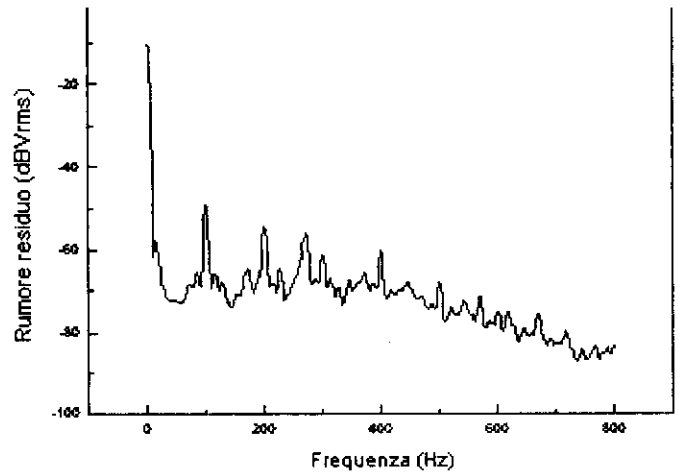

Figure 2.13: Spectrum of the cavity length fluctuations in the range 0-800 Hz

2.6 Optical Layout

The transfer optics of the laser beams @ 532 (green) and @1064 nm (IR) is formed of a collimating lens L_1 (see. Fig. 2.7) , followed by a Faraday insulator and a couple operating as an anamorphic lens for correcting the beal ellipticity. A dicroic mirror , placed in front of the cavity input plane, is used for overlapping the IR beam , collimated by means of lens L_3. The two overlapped beams are focused bthe lens L_2 toward the cavity.

The optical system can be described in the paraxial approximation by a sequence of ray matrices. We wiil indicatewith $\mathbf{M}_L$ the lens ray matrices , with $\mathbf{M}_P$ those relative to the prisms and with $\mathbf{M}_1$ the input mirror matrix. Q_x e Q_y indicate the complex curvature radii of the green light beam on the exit plane of the laser source, which is also chosen as origin of the coordinate z.

For a time dependece factor $\exp(-i\omega t)$ and a propagation toward the positive z-axis, the complex curvatureradius of a gaussian beam withwaist in z_w and confocal parameter b (> 0) is given by

$$Q(z) = z - z_w - ib$$

Q is related to the curvature radius R of the wavefront and to the spot size w by the relation

$$\frac{1}{Q} = \frac{1}{z - z_w - ib} = \frac{1}{R} + i\frac{2}{kw^2} \tag{2.20}$$

I fasci di ingresso al sistema sono caratterizzati dai seguenti parametri

wavelength	@532 nm	@1064 nm
exit spot-size $(1/e^2)$	0.7 mm	0.3 mm
exit beam divergence $(1/e^2)$	14 mrad	mrad
ellipticity	1.4:1	1.3:1

The far-field ellipticity is due to the different confocal parameters b_x e b_y,

$$\frac{w_x^2}{w_y^2} = \lim_{z \longrightarrow \infty} \frac{b_y}{b_x} \frac{(z_{fx} + z)^2 + b_x^2}{(z_{fy} + z)^2 + b_y^2} = \frac{b_y}{b_x}$$

On the other-hand the divergence is connected with the b-parameter bythe relation

$$\theta = 2\frac{w}{z} = 2\sqrt{\frac{2}{kb}} = 14 \times 10^{-3}\ rad$$

Then

$$\frac{b}{\lambda} = 6496 \longmapsto b = 3.456\ mm$$

D'altra parte, il fascio laser risulta ben collimato quando si pone ad una distanza di 80 mm una lente con f= 150 mm. Questo implica che il waist disti 70 mm dal piano d'uscita.

wavelength	@532 nm	@1064 nm
waist position	-70 mm	-50 mm
b_x	35 mm	18· mm
b_y	28 mm	16 mm
exit diameter $(1/e^2)$	0.7 mm	0.3 mm
exit divergence $(1/e^2)$	14 mrad	7 mrad
ellipticity	1.4:1	1.3:1

In conclusion the green beam on the exit plane has two different curvature complex radii respectively equal to

$$Q_x = 80 - i\,2.468\ ,\ Q_y = 80 - i\,4.838$$

The curvature radii relative to the wavefront on the inner face of the mirror M_1 will be obtained by applying the ABCD law,

$$Q'_x = \frac{A_x Q_x + B_x}{C_x Q_x + D_x}\ ,\ Q'_y = \frac{A_y Q_y + B_y}{C_y Q_y + D_y}$$

whose elements will be obtained by multiplying the following matrices

$$\begin{bmatrix} A_x & B_x \\ C_x & D_x \end{bmatrix} = \mathbf{M}_1 \cdot \mathbf{T}_{m-p} \cdot \underbrace{\mathbf{M}_{p,x} \cdot \mathbf{T}_{p-l}}_{prisms} \cdot \mathbf{M}_l \cdot \mathbf{T}_{l-0}$$

$$\begin{bmatrix} A_y & B_y \\ C_y & D_y \end{bmatrix} = \mathbf{M}_1 \cdot \mathbf{T}_{m-l} \cdot \mathbf{M}_l \cdot \mathbf{T}_{l-0}$$

Any misalignment of the prisms introduces a beam tilting $\theta_x = \Theta_p$ and a displacement X_p with respect to the optic axiss. Analogous effects are introduced by a mirror tilting.

Una volta calcolati i raggi di curvatura complessi Q_x e Q_y ed assumendo una dipendenza dal tempo del tipoAssuming a time dependence of the form $\exp(-i\omega t)$, the input beam on the inner face of the mirror is described by

$$u(x,y) = \exp\left(ik\left[\frac{(x-X)^2}{2Q_x} + \Theta_x x + \frac{(y-Y)^2}{2Q_y} + \Theta_y y\right]\right)$$

where X, Y e $\Theta_{x,y}$ represent the displacementsand the tiltings introduced by (a) focusing lens, (b) prisms, and (c) input mirror.

2.6.1 Offset and tilting of an optical component.

When the lens is displaced of the quantity δx and tilted by the angle θ_x the input vector modifies into

$$\begin{bmatrix} h \\ \alpha \end{bmatrix} \Rightarrow \begin{bmatrix} A & B \\ C & D \end{bmatrix} \cdot \left(\begin{bmatrix} h \\ \alpha \end{bmatrix} + \begin{bmatrix} -\delta h \\ -\delta\alpha \end{bmatrix}\right) + \begin{bmatrix} \delta h \\ \delta\alpha \end{bmatrix}$$

Consequently, the output ray will be displaced and tilted by thequantities

$$\begin{aligned} \delta h' &= -\delta h \cdot (A-1) - \delta\alpha \cdot B \\ \delta\alpha' &= -\delta h \cdot C - \delta\alpha \cdot (D-1) \end{aligned}$$

Introducing the vectors

$$\mathbf{V}_{(in)} = \begin{bmatrix} h \\ \alpha \end{bmatrix}\ ,\ \delta\mathbf{V} = \begin{bmatrix} \delta h \\ \delta\alpha \end{bmatrix}\ ,\ \delta\mathbf{V}' = \begin{bmatrix} \delta h' \\ \delta\alpha' \end{bmatrix}$$

we have

$$\delta\mathbf{V}' = -(\mathbf{M} - \mathbf{1}) \cdot \delta\mathbf{V}$$

Ray matrix of a biconvex matrix

For a biconvex lens with curvature radius R ad tickness Δ the ray matrix reads

$$\mathbf{M}_l = \begin{bmatrix} 1-\frac{\Delta}{R}\frac{n-1}{n} & \frac{\Delta}{n} \\ -2\frac{n-1}{R}+\frac{\Delta}{R^2}\frac{(n-1)^2}{n} & 1-\frac{n-1}{n}\frac{\Delta}{R} \end{bmatrix} \tag{2.21}$$

Ray matrix of two prisms

For a couple of prisms oriented as in Fig.(??).

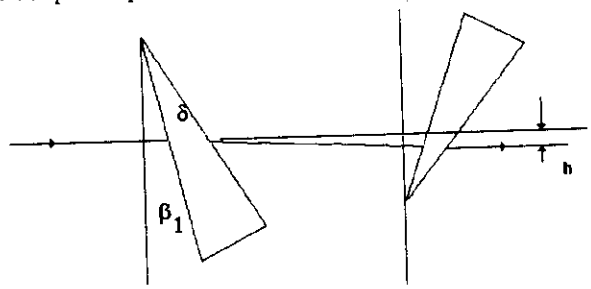

An anamorphic system used for correcting the asymmetry of the laser intensity distribution

the vector is modified as

$$\begin{bmatrix} h^{iv} \\ \alpha^{iv} \end{bmatrix} = \begin{bmatrix} A_p & B_p \\ 0 & A_p^{-1} \end{bmatrix} \cdot \begin{bmatrix} h \\ \alpha \end{bmatrix} + \begin{bmatrix} X_p \\ \Theta_p \end{bmatrix}$$

The vanishing of the element C implies

$$Q' = A_p^2 Q + A_p B_p$$

so that the confocal parameter is unaffected by the prisms.

,For analyzing the prism effects it is worth introducingthe functions

$$\begin{aligned} refr(\alpha,\beta,n) &= \arcsin\left[\frac{\sin(\alpha+\beta)}{n}\right]-\beta \\ g1(\alpha,\alpha',\beta) &= \frac{1-\tan(\alpha')\tan(\beta)}{1-\tan(\alpha)\tan(\beta)} \end{aligned}$$

The exit ray forms with the z-axis an angle α" and has an height h" respectively equal to

$$\begin{aligned} \alpha" &= prism(\alpha,\beta_1,\delta_1,n) \\ h" &= (h-x_{p1})g2(\alpha,\beta_1,\delta_1)+x_{p1} \end{aligned}$$

where

$$\begin{aligned} g2(\alpha,\beta,\delta) &= g1\left[refr(\alpha,\beta,n), prism(\alpha,\beta,\delta,n), \beta-\delta\right] g1\left[\alpha, refr(\alpha,\beta,n), \beta\right] \\ prism(\alpha,\beta,\delta,n) &= refr\left[refr(\alpha,\beta,n), \beta-\delta, \frac{1}{n}\right] \end{aligned}$$

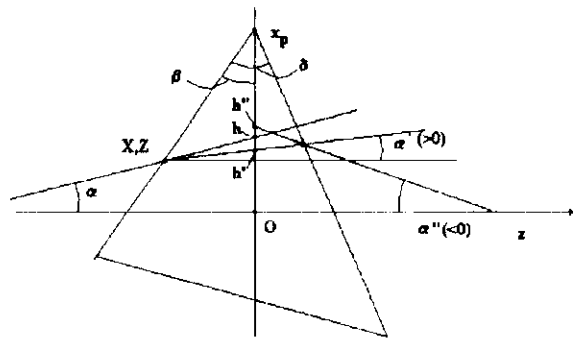

Figure 2.14: Geometry of a prism used in an anamorphic lens

Ray matrix of the input mirror

For the input plane-concave mirror of curvature radius R and tickness Δ the ray matrix reads

$$\mathbf{M}_1 = \begin{bmatrix} 1 & \frac{\Delta}{n} \\ \frac{n-1}{R} & 1+\frac{n-1}{n}\frac{\Delta}{R} \end{bmatrix}$$

Note that $f < 0$

Cavity ray matrix

With reference to Fig. (2.15)we easily obtain for the vector $\mathbf{V}$ transformed by the cavity

$$\begin{aligned} \mathbf{V}_{out} &= \delta\mathbf{V}_1 + \mathbf{R}_1\cdot\mathbf{T}_{13}\cdot\left[\delta\mathbf{V}'_{xtal} + \mathbf{T}_{34}\cdot\mathbf{T}_{42}\cdot\left[\delta\mathbf{V}_2 + \mathbf{R}_2\cdot\mathbf{T}_{24}\cdot\left(\delta\mathbf{V}_{xtal} + \mathbf{T}_{43}\cdot\mathbf{T}_{31}\cdot\mathbf{V}_{in}\right)\right]\right] \\ &= \mathbf{M}_{cav}\cdot\mathbf{V}_{in} + \delta\mathbf{V}_{cav} \end{aligned}$$

where

$$\begin{aligned} \delta\mathbf{V}_{xtal} &= -\delta\mathbf{V}'_{xtal} = \begin{bmatrix} \left(\frac{n-1}{n}\theta_{xtal} + \theta_{wo}\right)\ell_{xtl} \\ 0 \end{bmatrix} \\ \delta\mathbf{V}_2 &= \begin{bmatrix} 0 \\ 2\alpha_2 + \delta h_2\frac{2}{R_2} \end{bmatrix}, \ \delta\mathbf{V}_1 = \begin{bmatrix} 0 \\ 2\alpha_1 + 2\frac{\delta h_1}{R_1} \end{bmatrix} \end{aligned}$$

In conclusion,

$$\mathbf{M}_{cav} = \begin{bmatrix} 1-2\frac{\ell_{eff}}{R_2} & 2\ell_{eff}\left(1-\frac{\ell_{eff}}{R_2}\right) \\ -\frac{2}{R_1}-\frac{2}{R_2}\left(1-2\frac{\ell_{eff}}{R_1}\right) & \left(1-2\frac{\ell_{eff}}{R_1}\right)\left(1-2\frac{\ell_{eff}}{R_2}\right)-2\frac{\ell_{eff}}{R_1} \end{bmatrix}$$

and

$$\delta\mathbf{V}_{cav} = 2\begin{bmatrix} \left[-\frac{\ell_{xtl}}{R_2}\left(\theta_{xtal}\frac{n-1}{n}+\theta_{wo}\right)+\delta\alpha_2+\frac{\delta h_2}{R_2}\right]\ell_{eff} \\ \left[-\frac{\ell_{xtl}}{R_2}\left(\theta_{xtal}\frac{n-1}{n}+\theta_{wo}\right)+\delta\alpha_2+\frac{\delta h_2}{R_2}\right]\left(1-2\frac{\ell_{eff}}{R_1}\right)+\delta\alpha_1+\frac{\delta h_1}{R_1} \end{bmatrix}$$

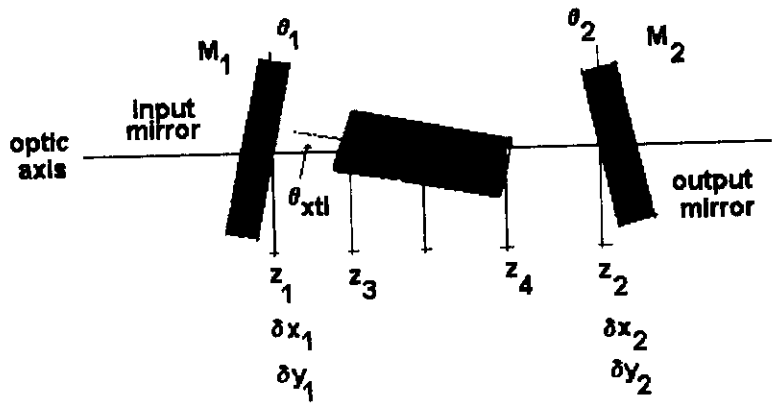

Figure 2.15: OPO cavity.. The tilting angles of the mirrors and crystal, indicated in figure, are negative.

where

$$\ell_{eff} = \ell_1 + \ell_2 + \frac{\ell_{xtl}}{n}$$

Tilting and displacement of the cavity gaussian modes

Per round-trip we have

$$\begin{aligned} h' &= A_{cav} h + B_{cav} \alpha + \delta h_{cav} \\ \alpha' &= C_{cav} h + D_{cav} \alpha + \delta \alpha_{cav} \end{aligned}$$

The complex curvature radius will be given by

$$Q = \frac{D_{cav} - A_{cav} \pm i\sqrt{4 - (A_{cav} + D_{cav})^2}}{2C_{cav}}$$

while

$$\begin{bmatrix} \delta h \\ \delta \alpha \end{bmatrix} = \frac{2}{\frac{\ell_{eff}}{R_2} + \frac{\ell_{eff}}{R_1} - \frac{\ell_{eff}}{R_1}\frac{\ell_{eff}}{R_2}} \begin{bmatrix} -2\frac{\ell_{eff}}{R_1} - \frac{\ell_{eff}}{R_2} + 2\frac{\ell_{eff}}{R_1}\frac{\ell_{eff}}{R_2} & 1 - \frac{\ell_{eff}}{R_2} \\ \frac{1}{R_1} + \frac{1}{R_2}\left(1 - 2\frac{\ell_{eff}}{R_1}\right) & -\frac{\ell_{eff}}{R_2} \end{bmatrix} \cdot \begin{bmatrix} \left\{-\frac{\ell_{xtl}}{R_2}\left(\theta_{xtal}\frac{n-1}{n} + \theta_{wo}\right) + \delta\alpha_2 + \frac{\delta h_2}{R_2}\right\}\ell_{eff} \\ \left\{-\frac{\ell_{xtl}}{R_2}\left(\theta_{xtal}\frac{n-1}{n} + \theta_{wo}\right) + \delta\alpha_2 + \frac{\delta h_2}{R_2}\right\}\left(1 - 2\frac{\ell_{eff}}{R_1}\right) + \delta\alpha_1 + \frac{\delta h_1}{R_1} \end{bmatrix}$$

2.7 Resonance frequencies and parametric gain

Inside the crystal placed at the center of the cavity thegreen field will be given by

$$u_{cav}(x, y; z) \propto \frac{1}{Q_{xtl}(z)} \exp\left(i n_g(T) k_g z + i n_g(T) k_g \frac{x^2 + y^2}{2Q_{xtl}(z)}\right)$$

where w(z) is related to Q(z) byEq. (2.20). In particular, at the crystal center

$$Q_{xtl}\left(z_{xtl}\right) = -ib_{xtl}$$

In general,

$$Q_{xtl}\left(z\right) = z - z_{xtl} - ib_{xtl}$$

Inside the cavity but outside the crystal

$$u_{cav}\left(x,y;z\right) \propto \frac{1}{Q_{cav}\left(z\right)} \exp\left(ik_g z + ik_g \frac{x^2+y^2}{2Q_{cav}\left(z\right)}\right)$$

beng

$$Q_{cav}\left(z_{xtl} - \frac{\ell_{xtl}}{2}\right) = \frac{1}{n_g} Q_{xtl}\left(z_{xtl} - \frac{\ell_{xtl}}{2}\right) = -\frac{\frac{\ell_{xtl}}{2} + ib_{xtl}}{n_g}$$

$Q_{cav}\left(z_1\right)$ may be calculated by means of Eq. (??). Therefore

$$-ib_{xtl} = n_g\left(Q + \ell_1\right) + \frac{\ell_{xtl}}{2}$$

Finally, the ratio between the fields on the two mirrors is given by

$$\frac{u_{cav}\left(x,y;z_2\right)}{u_{cav}\left(x,y;z_1\right)} = \exp\left[ik_g\left(\ell_1 + \ell_2\right) + ik_g n_g \ell_{xtl} - i2\Psi\right]$$

where

$$2\Psi = \arg\left\{Q_{cav}\left(z_2\right)\right\} - \arg\left\{Q_{cav}\left(z_1\right)\right\}$$

For a symmetric cavity

$$Q_{cav}\left(z_2\right) = -Q^*_{cav}\left(z_1\right) \Rightarrow 2\Psi = -2\arg Q_{cav}\left(z_1\right) - \pi$$

At the cavity resonances at 532 nm and 1064 nm we have

$$\begin{aligned} m_g\pi &= k_g\left(\ell_1 + \ell_{2g} + n_g\left(T\right)\ell_{xtl}\right) - 2\Psi \\ m_{IR}\pi &= \frac{1}{2}k_g\left(\ell_1 + \ell_{2IR} + n_{IR}\left(T\right)\ell_{xtl}\right) - 2\Psi \end{aligned}$$

2.8 Temperature and length constraints for degenerate operation

In general the difference between the longitudinal modal indices of the green and IR resonances is related to the cavity lenghts and to the temperature throughthe relation

$$m_g - 2m_{IR} = k_g\left(\ell_{2g} - \ell_{2IR}\right) + \frac{k_g \ell_{xtl}}{\pi}\left(n_g\left(T\right) - n_{IR}\left(T\right)\right) + \frac{2\Psi}{\pi}$$

For a degenerate configuration[18] it must be

degenerate configuration

$$\ell_{2g} = \ell_{2IR}$$

so that for achiving a degenerate configuration we must have

$$m_g - 2m_{IR} = \frac{k_g \ell_{xtl}}{\pi}\left(n_g(T) - n_{IR}(T)\right) + \frac{2\Psi}{\pi}$$

The phase $\Psi\,(<\pi/2)$ is given by

$$\Psi = -\frac{\pi}{2} - \arg Q = -\frac{\pi}{2} + \arctan\frac{2R}{k_g w_g^2}$$

Consequently

$$m_g - 2m_{IR} + 1 = \frac{k_g \ell_{xtl}}{\pi}\left(n_g(T) - n_{IR}(T)\right) + \frac{2}{\pi}\arctan\frac{2R}{k_g w_g^2}$$

For $R = 150\ mm$ and $w_g = 1\ mm$ the *condition for degenerate operation* reads

$$m_g - 2m_{IR} + 1 = \frac{k_g \ell_{xtl}}{\pi}\left(n_g(T) - n_{IR}(T)\right) + \frac{0.15}{\pi^2}$$

On the other hand the OPO gain is proportional to

$$g(\sigma,\varsigma) \propto \frac{1}{\varsigma}\mid \Im\left[e^{i\phi_g + i\phi_{IR}}\int_{-\varsigma}^{\varsigma}\frac{e^{i\sigma x}}{1+ix}dx\right]\mid^2$$

where

$$\begin{aligned}\varsigma &= \frac{l_{xtl}}{b_{xtl}}\ ,\ \sigma = k_g b_{xtl}\left(n_g(T) - n_{IR}(T)\right)\\ b_{xtl} &= -n_g\Im(Q) = n_g R\frac{\frac{2R}{k_g w_g^2}}{1+\left(\frac{2R}{k_g w_g^2}\right)^2}\end{aligned}$$

gain at zero detuning

In particular, we can ignore the term $\frac{0.15}{\pi^2}$. In addition for $\sigma = 0$

$$\begin{aligned}g(0,\varsigma) &\propto \frac{1}{\varsigma}\mid \Im\left[e^{i\phi_g + i2\phi_{IR}}\int_{-\varsigma}^{\varsigma}\frac{1}{1+ix}dx\right]\mid^2\\ &= \frac{1}{\varsigma}\left(\pi - 2\arctan\frac{1}{\varsigma}\right)^2\sin^2\left(\phi_g + 2\phi_{IR}\right)\end{aligned}$$

2.9 Amplitudes of the modes excited in the cavity

Consideriamo un fascio di ingresso alla cavita' descritto sulla faccia interna dello specchio M_1 dall'espressione

$$u_{in}(x,y) = \frac{2}{\sqrt{w_x w_y \pi}}\exp\left(ik\left[\frac{(x-X)^2}{2Q_x} + \Theta_x x + \frac{(y-Y)^2}{2Q_y} + \Theta_y y\right]\right)$$

ed un modo in cavita' della forma

$$u_{cav}(x,y) = \frac{2}{w\sqrt{\pi}}\exp\left(ik\left[\frac{(x-X_{cav})^2}{2Q_{cav}} + \Theta_{(cav)x}x + \frac{(y-Y_{cav})^2}{2Q_{cav}} + \Theta_{(cav)y}y\right]\right)$$

litudes

The amplitude of the mode $TEM_{\ell m}$ will be given by

$$\begin{aligned} C_{\ell m} &= \frac{4}{\pi w\sqrt{w_x w_y}}\frac{1}{\sqrt{2^{\ell+m}\ell!m!}} \\ &\times\int dx\int dy\exp\left(ik\left[\frac{(x-\Delta X)^2}{2Q_x}+\frac{(y-\Delta Y)^2}{2Q_y}-\frac{x^2+y^2}{2Q^*_{cav}}+\Delta\Theta_x x+\Delta\Theta_y y\right]\right) \\ &\times H_\ell\left(\sqrt{2}\frac{x}{w}\right)H_m\left(\sqrt{2}\frac{y}{w}\right) \end{aligned}$$

where

$$\begin{aligned} \Delta X &= X - X_{cav}\ ,\ \Delta Y = Y - Y_{cav} \\ \Delta\Theta_x &= \Theta_x - \Theta_{(cav)x}\ ,\ \Delta\Theta_y = \Theta_y - \Theta_{(cav)y} \end{aligned}$$

Putting

$$a = ik\left(\frac{1}{Q^*_{cav}}-\frac{1}{Q_x}\right)\ ,\ b = k\left(\Delta\Theta_x-\frac{\Delta X}{Q_x}\right)\ ,\ c = \exp\left[ik\frac{\Delta X^2}{2Q_x}\right]$$

we have

$$C_\ell = \frac{1}{\sqrt{2^\ell\ell!}}H_l\left(i\frac{\sqrt{2}\frac{bw}{aw^2}}{\sqrt{1-\frac{4}{aw^2}}}\right)C_0$$

where

$$C_0 = \left[\frac{Q_xQ^*_{cav}}{Q^*_xQ_{cav}}\frac{(Q_{cav}-Q^*_{cav})(Q_x-Q^*_x)}{(Q_x-Q^*_{cav})^2}\right]^{1/4}\exp\left(i\frac{k}{2}\left[\frac{\Delta X^2}{Q_x}-\frac{Q_xQ^*_{cav}}{Q_x-Q^*_{cav}}\left(\Delta\Theta_x-\frac{\Delta X}{Q_x}\right)^2\right]\right)$$

For $b=0$ we have

$$C_{2\ell} = \frac{(-1)^\ell 2^\ell(2\ell-1)!!}{\sqrt{2^\ell\ell!}}C_0$$

Combining the contributions of the two axes

$$\begin{aligned} C_{tot} &= \sqrt{\frac{Q^*_{cav}}{Q_{cav}}\frac{Q_{cav}-Q^*_{cav}}{(Q_x-Q^*_{cav})(Q_y-Q^*_{cav})}\sqrt{\frac{Q_xQ_y}{Q^*_xQ^*_y}(Q_x-Q^*_x)(Q_y-Q^*_y)}} \\ &\times\exp\left(i\frac{k}{2}\left[\frac{X^2}{Q_x}-\frac{Q_xQ^*}{Q_x-Q^*}\left(\Delta\Theta_x-\frac{\Delta X}{Q_x}\right)^2+\frac{\Delta Y^2}{Q_y}-\frac{Q_yQ^*}{Q_y-Q^*}\left(\Delta\Theta_y-\frac{\Delta Y}{Q_y}\right)^2\right]\right) \end{aligned}$$

Ignoring tilting and misalignments

$$|C_{tot}|^2 = 4\sqrt{\frac{b^2_{cav}b_xb_y}{\left[(b_x+b_{cav})^2+(z_x-z_{cav})^2\right]\left[(b_y+b_{cav})^2+(z_y-z_{cav})^2\right]}}$$

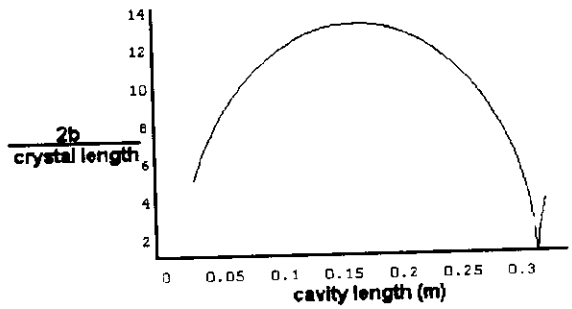

Figure 2.16:

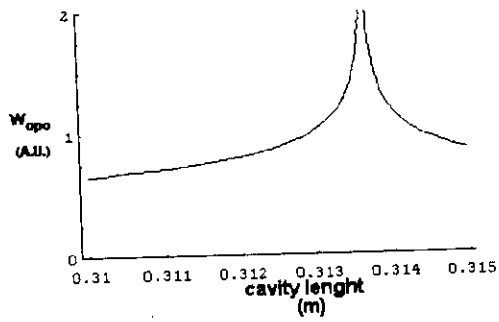

Figure 2.17:

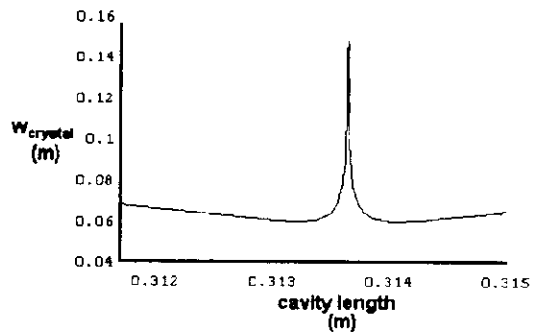

Figure 2.18:

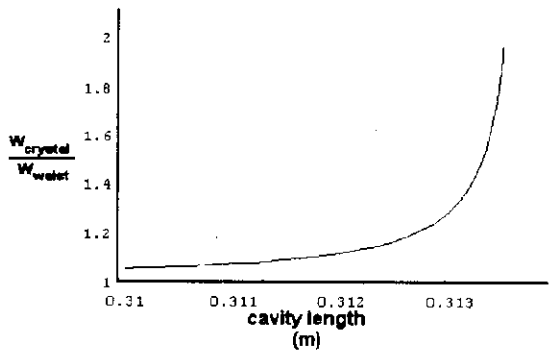

Figure 2.19:

Bibliography

[1] R. Loudon and P. L. Knight. Squeezed light. *J. Modern Optics*, 34:709, 1987. teorico , rassegna.

[2] D. F. Walls G. J. Milburn and H. J. Carmichael. *Optica Acta*, 29:1179, 1982.

[3] H. P. Yuen and J. H. Shapiro. *IEEE Trans. Inf. Theory*, 24:657, 1978.

[4] H. P. Yuen and J. H. Shapiro. *IEEE Trans. Inf. Theory*, 26:78, 1980.

[5] J. H. Shapiro H. P. Yuen and J. A. Machado Mata. *IEEE Trans. Inf. Theory*, 25:179, 1979.

[6] H. P. Yuen and V. W. S. Chan. Noise in homodyne and heterodyne detection. *Opt. Lett.*, 8:177, 1983.

[7] S. Machida and Y. Yamamoto. Quantum-limited operation of balanced mixer homodyne and hterodyne receivers. *IEEE J.Q.E.*, QE22:617, 1986.

[8] J. H. Shapiro and S. S. Wagner. Phase and amplitude uncertainties in heterodyne detection. *IEEE J.Q.E.*, QE20:803, 1984.

[9] A. Yariv and P. Yeh. *Optical Waves in Crystals*. J. Wiley and Sons, New York, 1984.

[10] J. Jerphagnon S. K. Kurtz and M. M. Choy. *Nonlinear Dielectric Susceptibilities*, volume 11 of *Landolt-Bornstein*. Springer-Verlag, Berlin, 1979. Landolt-Bornstein.

[11] A. Yariv. *Quantum Electronics*. J. Wiley and Sons, New York, 1987.

[12] W. J. Kozlovsky R. Byer R. C. Eckardt, C. D. Nabors. Optical parametric oscillator frequency tuning and control. *J.O.S.A. B*, 8:646, 1991.

[13] G.D. Boyd and D.A. Kleimann. Parametric interaction of focused gaussian light beams. *J. Appl. Physics*, 39:3597, 1968.

[14] Min Xiao Lin-An Wu and H.J. Kimble. Squeezed state of light from an optical parametric oscillator. *J. Opt. Soc. Am. B*, 4:1465, 1987.

[15] M. J. Collett and C. W. Gardiner. Squeezing of intracavity and traveling-wave light fields produced in parametric amplification. *Phys. Rev. A*, 30(3):1386–1391, Sep. 1984. recent calculations by Milburn and Walls and

by Yurke have shown that squeezing in a parametric amplifier is a subject of great subtlety . Milburn and Walls madecalculations using master-equation techniques. The approach presented in this paper povides a method for linking the internal field with the input by identification of the "noise" with the incoming field, and the output is then calculated using the boundary conditions at the cavity mirrors.

[16] M. J. Collett and D. F. Walls. Squeezing spectra for nonlinear optical systems. *Phys. Rev. A*, 32(5):2887–2892, Nov. 1985.

[17] C. W. Gardiner and C.M. Savage. *Opt. Commun.*, 50:173, 1984.

[18] E. Giacobino T. Debuisschert, A. Sizmann and C. Fabre. Type ii continuous wave optical parametric oscillators: oscillation and frequency tuning characteristics. *J. Opt. Soc. Am. B*, 10:1668, 1993.

[19] A. Porzio R. Romano S. Solimeno M. Fiorentino, P. Maddalena. *Opt. Commun.*, 1996.

[20] L. Di Fiore F. Fusco A. Grado L. Milano F. Barone, R. De Roasa and G.. Russo. Real tiem digital control of optical interferometers by mechanical modulation techniques. *Appl. Optics*, 33:7846, 1994.

[21] T. W. Hansch and B. Couillaud. Laser frequency stabilization by polarization spectroscopy. *Optics Communications*, 35:441, 1980.

[22] F. W. Kovalski J. Hough G. M. Ford A. J.. Munley R. W. P. Drever, J. L. Hall and H. Ward. Laser phase and frequency stabilization using an optical resonator. *Appl. Phys. B*, 31:97, 1983.

Chapter 3

Interferometric detection of gravitational waves and squeezed radiation

3.1 Introduction

In interferometric measurements the quantum noise is originated by the fluctuations of the number of photons at the detector. Near the zeroth-order minimum of interference the noise is approximately independent of the amplitude and phase noise of the input field (say $a_{(1)}$) at port P_1. Rather the noise is due to fluctuations of the component of the vacuum field (say $a_{(2)}$) at port P_2, which is 90^0 out of phase with $a_{(1)}$. An additional component comes in when the intensity is so large to make the fluctuating action of the radiation pressure on the mirrors no more negligible [1]. As a consequence of the opposite dependence on the intensity of the photon and radiation pressure noises, the sensitivity of an ideal interferometer reaches its best value for an optimal value of the intensity of the illuminating beam.

For a vacuum field at the unused port P_2 the optimal power of the input laser comes out to be quite large and of no experimental interest. To reduce considerably this value Caves [1] suggested to squeeze the vacuum field. In fact, the photon noise can be reduced by squeezing the fluctuations in the 90^0 out of phase component of $a_{(2)}$. As pointed out by Caves , Gea-Banacloche and Leuchs[2][3][4] the advantages of such a brilliant solution are drastically reduced by the imperfections of the interferometer. Among these are non equal losses in both arms, wavefront distortions, depolarization and imperfect overlap between the two beams. T

For what concerns the detection apparatus most antennas extract the GW signal by manipulating in a suitable way the spectral density of the output (i.e. the Fourier transform of the autocorrelation). Two methods have been proposed to optimize the response of the interferometer: phase modulation technique [5] and the balanced detection in which the difference between the detected photons at the output ports is measured around a zero working point[6][7][8][9].

3.2 Quantum input-output theory of a Michelson interferometer

In the Michelson interferometer (Fig.1) we have two input fields entering through ports P_i, $i = 1, 2$, described by the operators $(a_i,\ a_i^\dagger)$. To them correspond two

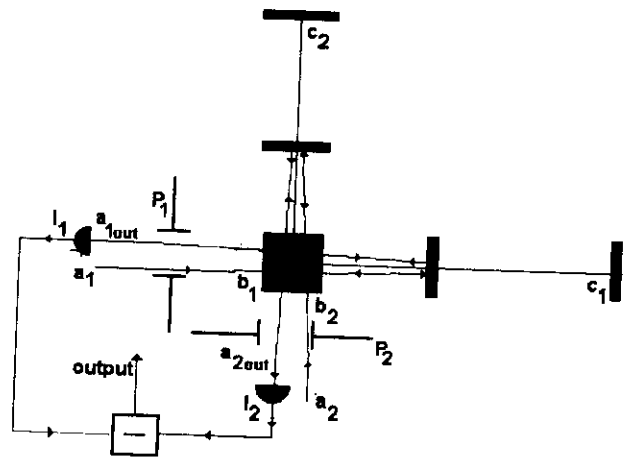

Figure 3.1: Schematic of a Michelson interferometer with suspended Fabry-Perot cavities in the two arms

fields at the mirrors M_i described by $(b_i,\ b_i^\dagger)$ and two output fields at P_i described by $(c_i,\ c_i^\dagger)$. We simplify the Michelson interferometer as a device with two arms at the end of wich two outer mirrors M_i are attached to some strings, thus behaving as two pendula, without considering Fabry-Perot cavities and beam delaying optics into these arms. The position of the mirrors are controlled by the joint action of the restoring forces and the radiation pressure [10]. We will suppose that in all processes the dissipative and active effects are negligible so that conservation of energy is ensured.

The Hamiltonian in $\mathcal{H}^\rho$ is taken to be

$$\mathcal{H}^\rho = \hbar\omega(\rho_1^\dagger\rho_1 + \rho_2^\dagger\rho_2) \tag{3.1}$$

with ω the frequency and $\hbar$ the Planck's constant. Implicit here is the assumption of equal frequencies for the mode 1 and 2. This can be achieved by introducing some degree of interaction among the two modes, which anyhow can be ignored in a first approximation, [?]. The operators are connected each other by 2×2 unitary matrices, the elements of which depend on the physical and geometrical parameters of the interferometer[11]

$$b = Va, \qquad b^\dagger = a^\dagger V^\dagger$$

where

$$a = \begin{bmatrix} a_1 \\ a_2 \end{bmatrix} \quad ; \quad b = \begin{bmatrix} b_1 \\ b_2 \end{bmatrix}$$

$$a^\dagger = \begin{bmatrix} a_1^\dagger & a_2^\dagger \end{bmatrix} \quad ; \quad b^\dagger = \begin{bmatrix} b_1^\dagger & b_2^\dagger \end{bmatrix}$$

We conveniently write

$$V = \Phi \cdot K$$

with

$$\Phi = \begin{bmatrix} e^{i\phi_1} & 0 \\ 0 & e^{i\phi_2} \end{bmatrix}$$
$$K = \begin{bmatrix} \alpha_1 & \beta_2 \\ \beta_1 & \alpha_2 \end{bmatrix}$$

In the above α_i and β_i are the complex transmitivity and reflectivity parameters of the beam splitter (BS) arbitrarily oriented for the i-th input field mode respectively. ϕ_i are the phase distance between BS and the mirror M_i. Also

$$c = Ua \quad ; \quad c^\dagger = a^\dagger U^\dagger \tag{3.2}$$

and

$$U = -K^T \Phi^2 K \tag{3.3}$$

Thus all the information about influence of the optical elements of the interferometer on the light acting on the mirrors is contained in the unitary matrix V described in generic case by four independent parameters. The influence of the interferometer elements (beam splitter, mirrors, etc.,) on the outgoing field is described by the unitary matrix U which in the case under consideration is completely determined by the matrix V.

If we consider a $50-50\%$ BS, then the elements of the matrix K are

$$\alpha_1 = \alpha_2 = \frac{e^{i\delta}}{\sqrt{2}}$$
$$\beta_1 = \beta_2 = \frac{e^{i\mu}}{\sqrt{2}} \tag{3.4}$$

where δ is the phase introduced by the BS which can be set to zero for an ideally thin BS while μ is the phase introduced by the BS between the reflected and transmitted waves and for simplicity we take $\mu = \pi/2$. Then

$$V = \frac{1}{\sqrt{2}} \begin{bmatrix} e^{i\phi_1} & ie^{i\phi_1} \\ ie^{i\phi_2} & e^{i\phi_2} \end{bmatrix} \tag{3.5}$$

and

$$U = -\frac{1}{\sqrt{2}} \begin{bmatrix} e^{2i\phi_1} - e^{2i\phi_2} & ie^{i\phi_1} + ie^{2i\phi_2} \\ ie^{2i\phi_1} + ie^{2i\phi_2} & -e^{2i\phi_1} + e^{2i\phi_2} \end{bmatrix} \tag{3.6}$$

In addition,

$$V^\dagger \cdot \sigma_3 \cdot V = -\sigma_2 \tag{3.7}$$

with σ_2 the Pauli spin matrix and

$$U^\dagger \cdot \sigma_3 \cdot U = \begin{bmatrix} -\cos\phi & -\sin\phi \\ -\sin\phi & \cos\phi \end{bmatrix} \tag{3.8}$$

with $\phi = 2(\phi_2 - \phi_1)$.

For the interferometer operating on a dark fringe ($\phi = \delta\phi + (2n+1)\pi/2$) and for small values of $\delta\phi$

$$U^\dagger \cdot \sigma_3 \cdot U = \sigma_1 + \delta\phi\ \sigma_3 \tag{3.9}$$

$\delta\phi$ is given by the sum of the GW signal $\delta\phi_{GW}$ and the noise term $\delta\phi_N$ due to: (i) noise transmitted to the mirrors through the suspensions, (ii) vibration modes of the mirrors, (iii) pressure fluctuations in the partially evacuated pipes forming the interferometer arms, and (iv) radiation pressure noise,

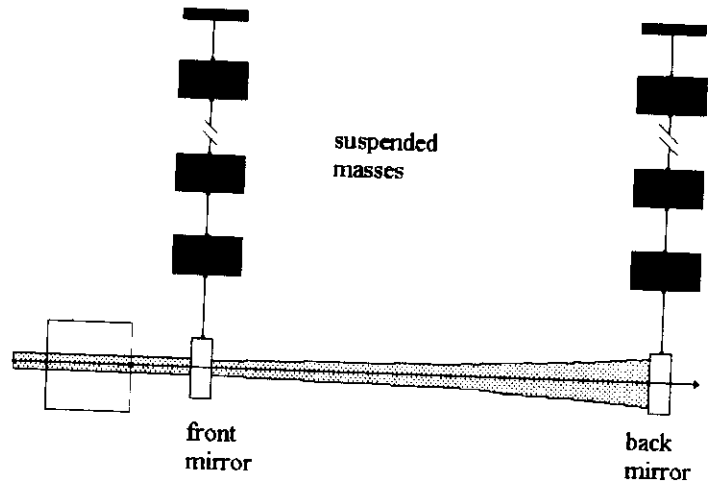

Figure 3.2: Schematic of the multiple pendula used for reducing the seismic noise in the VIRGO GW antenna

3.3 Multimode Michelson interferometer

We can analyze the interferometer by exploiting a multimode representation of the beams

$$\begin{aligned} E^{(+)}_{(x)}(\mathbf{r}) &= \sum_j a_{(x)j} u_{(x)j}(y,z;x) \\ E^{(+)}_{(y)}(\mathbf{r}) &= \sum_j a_{(y)j} u_{(y)j}(x,z;y) \end{aligned} \tag{3.10}$$

Accordingly, the beams will be represented by the two-dimension vector

$$\mathcal{A} = \begin{bmatrix} \mathbf{A}_{(1)} \\ \mathbf{A}_{(2)} \end{bmatrix}$$

having for components the N-dimension vectors

$$\mathbf{A}_{(1)} = \begin{bmatrix} a_{(x)0} \\ \vdots \\ a_{(x)N-1} \end{bmatrix} \quad , \quad \mathbf{A}_{(2)} = \begin{bmatrix} a_{(y)0} \\ \vdots \\ a_{(y)N-1} \end{bmatrix} \tag{3.11}$$

In case of misalignment and mismatching of these two beams with respect to the modes of the interferometer $\mathcal{A}_{(in)}$ is transformed by the matrix $\mathcal{M}_{(in)}$, $\mathcal{A} = \mathcal{M}_{(in)} \cdot \mathcal{A}_{(in)}$

The beams propagate toward the beam splitter BS where they are represented by the vector $\mathcal{A}' = T' \cdot \mathcal{A}$

The beams undergo some aberrations at the passage through the beamsplitter as a consequence of (i) deviation from planarity of the surfaces, (ii) inhomogeneities and (iii) irregularities of the splitting multilayer. We will describe these effects by imagining the beam-splitter sandwitched among four transparencies on the four faces represented by the unitary transformations (see Fig. (3.3)), .

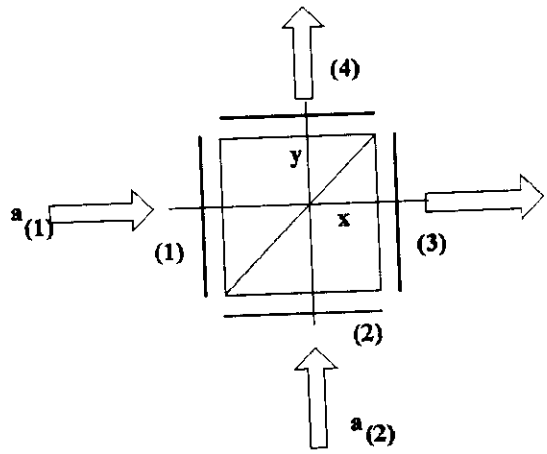

Figure 3.3: Schematic of the transparencies used for simulating the beam-splitter aberrations

3.3.1 Cavity reflection

Now, we have to pay particular attention to the response of the cavities to the different mode, described by the diagonal matrix

$$\mathcal{T}_{(cav)} = \begin{bmatrix} \Upsilon_{(1)} & 0 \\ 0 & \Upsilon_{(2)} \end{bmatrix} \tag{3.12}$$

with

$$\Upsilon_{(i)} = \begin{bmatrix} \tilde{r}_{(i)0} & 0 & 0 \\ 0 & \tilde{r}_{(i)1} & 0 \\ \vdots & \vdots & \ddots \end{bmatrix} \tag{3.13}$$

$\tilde{r}_{(i)j}$ describing the reflection of the j-th mode. For sake of simplicity we assume that only the fundamental mode resonates with the cavities.

Fundamental mode

For obtaining the operators $\tilde{r}_{(i)0}$ we have to analyze the respone of the cavities to the fundamental modes. Following Pace et al. [12] the dynamics of the TEM_{00} mode amplitude c inside either one cavity by means of the quantum Langevin equation

Radiation pressure

Since the mirrors are suspended to multiple pendula, $\Delta_{(rp)}$ can be represented as a superposition of normal modes,

$$\Delta_{(rp)} = \sum_m \left(d_m b_m + d_m^* b_m^\dagger \right) \tag{3.14}$$

with the annihilation operator b_m of the m-th mode satisfying a quantum Langevin equation,

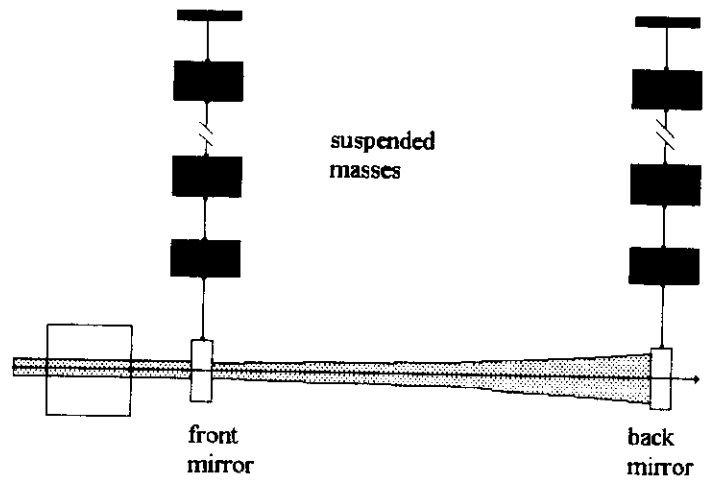

Figure 3.4: Schematic of the super-attenuators used for reducing the seismic noise transmitted to the cavity mirrors

Introducing the Green's function $\Gamma_m(t) = \exp[-(i\Omega_m + \frac{1}{2}\gamma_m)t]$, the integral of the last equation can be written as

$$b_m = -i\kappa_m \Gamma_m * cc^\dagger + \sqrt{\gamma_m} b_{(in)m} \tag{3.15}$$

with * representing the convolution operator.

3.3.2 Output fields

3.4 Interferometer output

We choose as interferometer output the difference I between the photocurrents detected at ports 1 and 2 respectively . So that if we indicate by η_i the quantum efficiency of the i-th detector and put $\eta_1 = \eta + \delta\eta, \eta_2 = \eta - \delta\eta$ we have

$$\begin{aligned} I &= \int_{S_1} E_1^{(-)}(\mathbf{r};t) E_1^{(+)}(\mathbf{r},t) d\mathbf{r} - \int_{S_2} E_2^{(-)}(\mathbf{r};t) E_2^{(+)}(\mathbf{r},t) d\mathbf{r} \\ &= \sum_i (\eta_1 d_{i_1}^\dagger d_{i_1} - \eta_2 d_{i_2}^\dagger d_{i_2}) = \eta \mathcal{D}^\dagger \cdot \sigma_3 \cdot \mathcal{D} + \delta\eta \mathcal{D}^\dagger \cdot \sigma_0 \cdot \mathcal{D} \end{aligned}$$

In conclusion, the interferometer output will be represented by

$$I = \alpha_0 A_0 + I_{(pn)} A_{(pn)} + (\delta\phi_{(GW)} + \delta\phi_{(sus)} + \delta\phi_{(mir)} + \delta\phi_{(pre)} + \delta\phi_{(rp)}) A_3 \tag{3.16}$$

with $A_i = \mathbf{a}^\dagger \cdot \sigma_i \cdot \mathbf{a}$ and $A_{\phi_{(pn)}} = \cos\phi_{(pn)} A_1 - \sin\phi_{(pn)} A_2$. $I_{(pn)}$ and $\phi_{(pn)}$ are defined by the relations $I_{(ab)} \cos\phi_{(pn)} = \cos\phi' + \alpha_1$ and $I_{(ab)} \sin\phi_{(pn)} = \sin\phi' - \alpha_2$

In Fig. 3 we have plotted a typical sensitivity curve of a GW antenna. The low-frequency part represents mostly the frequency response of the multiple pendula suspension for the mirrors.

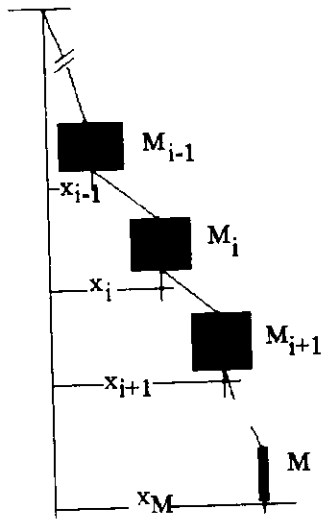

Figure 3.5: Geometry of a superattenuator consisting of several suspended masses

3.5 Autocorrelation of the interferometer output

In GW antennas the signal is extracted from the frequency spectrum of the photocurrent, that is from the Fourier transform of the autocorrelation

$$\begin{aligned} C(t) &= \int_{S_1} dr' \int_{S_1} dr'' < E^{(-)}_{(out)1}(r';0) E^{(-)}_{(out)1}(r'';t) E^{(+)}_{(out)1}(r'';t) E^{(+)}_{(out)1}(r';0) > \\ &+ \int_{S_2} dr' \int_{S_2} dr'' < E^{(-)}_{(out)2}(r';0) E^{(-)}_{(out)2}(r'';t) E^{(+)}_{(out)2}(r'';t) E^{(+)}_{(out)2}(r';0) > \\ &- \int_{S_1} dr' \int_{S_2} dr'' < E^{(-)}_{(out)1}(r';0) E^{(-)}_{(out)2}(r'';t) E^{(+)}_{(out)2}(r'';t) E^{(+)}_{(out)1}(r';0) > \\ &- \int_{S_2} dr' \int_{S_1} dr'' < E^{(-)}_{(out)2}(r';0) E^{(-)}_{(out)1}(r'';t) E^{(+)}_{(out)1}(r'';t) E^{(+)}_{(out)2}(r';0) > \\ &\equiv <: I, I :> \end{aligned} \tag{3.17}$$

with : ... : indicating time- and normal-ordered sequences.

Next, using Eq. (3.16) yields

$$\begin{aligned} C(t) &= [C_{(GW)}(t) + C_{(sus)}(t) + C_{(mir)}(t) + C_{(pre)}(t) + C_{(rp)}(t)] <: A_3, A_3 :> \\ &+ < : (\alpha_0 A_0 + I_{(pn)} A_{\phi_{(pn)}}), (\alpha_0 A_0 + I_{(pn)} A_{\phi_{(pn)}}) :> \end{aligned} \tag{3.18}$$

Consequently the power spectrum of the interferometer output will be given by

$$\begin{aligned} \mathcal{F}(\omega) &= [\mathcal{F}_{GW}(\omega) + \mathcal{F}_{(sus)}(\omega) + \mathcal{F}_{(mir)}(\omega) + \mathcal{F}_{(pre)}(\omega) + |H_M(\omega)|^2 \mathcal{F}_{\phi'}(\omega)] \star \mathcal{F}_3(\omega) \\ &+ \mathcal{F}_{(pn)}(\omega) \end{aligned} \tag{3.19}$$

having indicated by $\mathcal{F}_{(pn)}(\omega)$ the Fourier transform of the autocorrelations of $\alpha_0 A_0 + I_{(pn)} A_{\phi_{(pn)}}$ and by H_M the Fourier transform $\mathcal{F}_\omega\{\Gamma_M(t)\}$ of the mirror suspension.

This expression exhibits the typical features of the GW antenna sensitivity. There is a contribution independent of the laser intensity, which is a function of the suspension, mirror a pipe pressure fluctuations. Next there is the contribution of the optical aberration which decreases with the laser intensity. Finally, we have the terms depending on the photon noise and on the radiation pressure fluctuations. While in absence of radiation pressure effects the photon noise contribution decreases by increasing the intensity, the radiation pressure effect is an increasing function of the laser intensity. Since the frequency response of the mirror suspension system decays rapidly with the frequency, we can neglect the contribution of the radiation pressure noise alone, by retaining only the mixed terms.

In order to estimate the sensitivity of the GW antenna we can assume as minimum detectable signal the quantity

$$h(\omega) = \mathcal{F}_{(sus)}(\omega) + \mathcal{F}_{(mir)}(\omega) + \mathcal{F}_{(pre)}(\omega) + |H_M(\omega)|^2 \mathcal{F}_{\phi'}(\omega)] \star \mathcal{F}_3(\omega) + \frac{\mathcal{F}_{(pn)}(\omega)}{A_3^2} \tag{3.20}$$

Bibliography

[1] C. M. Caves. Quantum-mechanical noise in an interferometer. *Phys. Rev. D*, 23:1693, 1981. teoria dell'interferometro con radiazione squezed.

[2] J. Gea-Banacloche and G.. Leuchs. *J. Opt. Soc. Am. B*, 4:1667, 1987. interferometri, rad. squeezed, limiti realizzativi.

[3] J. Gea-Banacloche and G. Leuchs. *J. Modern Optics*, 34:793, 1987.

[4] J. Gea-Banacloche and G. Leuchs. Squeezed states in non-ideal interferometers: the effect of aberrations. *J. of Modern Optics*, 36(10):1277–1284, Oct. 1989. teorico.

[5] L. Schnupp W. Winkler K. Maischberger D. Shoemaker, R. Schilling and A. Rudiger. *Phys. Rev. D*, 38:423, 1988.

[6] A. Brillet. *Ann. Phys. (Paris)*, 10:219, 1985.

[7] L. Schnupp W. Winkler H. Billing A. Rudiger, R. Schilling and K. Maischberger. Gravitation wave detection by laser interferometry. Technical Report MPQ Report-68, Max Planck fur Quantenoptik, 1983.

[8] W. G. Unruh. *Quantum Optics Experimental Gravitation and Measurement Theory*, page 647. Plenum Press, New York, 1983.

[9] M. T. Jackel and S. Reynaud. *Europhysics Lett.*, 13:301, 1991.

[10] C. De Lisio L. Di Fiore L. Milano S. Solimeno, F. Barone and G. Russo. *Phys. Rev. A*, 43:6227, 1991.

[11] M. A. Man'ko V. I. Man'ko S. Solimeno N. A. Ansari, L. Di Fiore and F. Zaccaria. Quantum limits in interferometric gravitational-wave antennas in the presence of even and odd coherent states. *Phys. Rev. A*, 49(3):2151–2156, March 1994.

[12] D. F. Walls A. F. Pace, M. J. Collett. *Phys. Rev. A*, 47:3173, 1993.